Department of Precision and Microsystems Engineering

Planar approach for designing and fabricating active metamaterials

Kees de Jong

Report no : 2022.043
Coach : Dr. Andres Hunt
Professor : Dr. Andres Hunt
Specialisation : MNE
Type of report : Thesis
Date : 31 August 2022

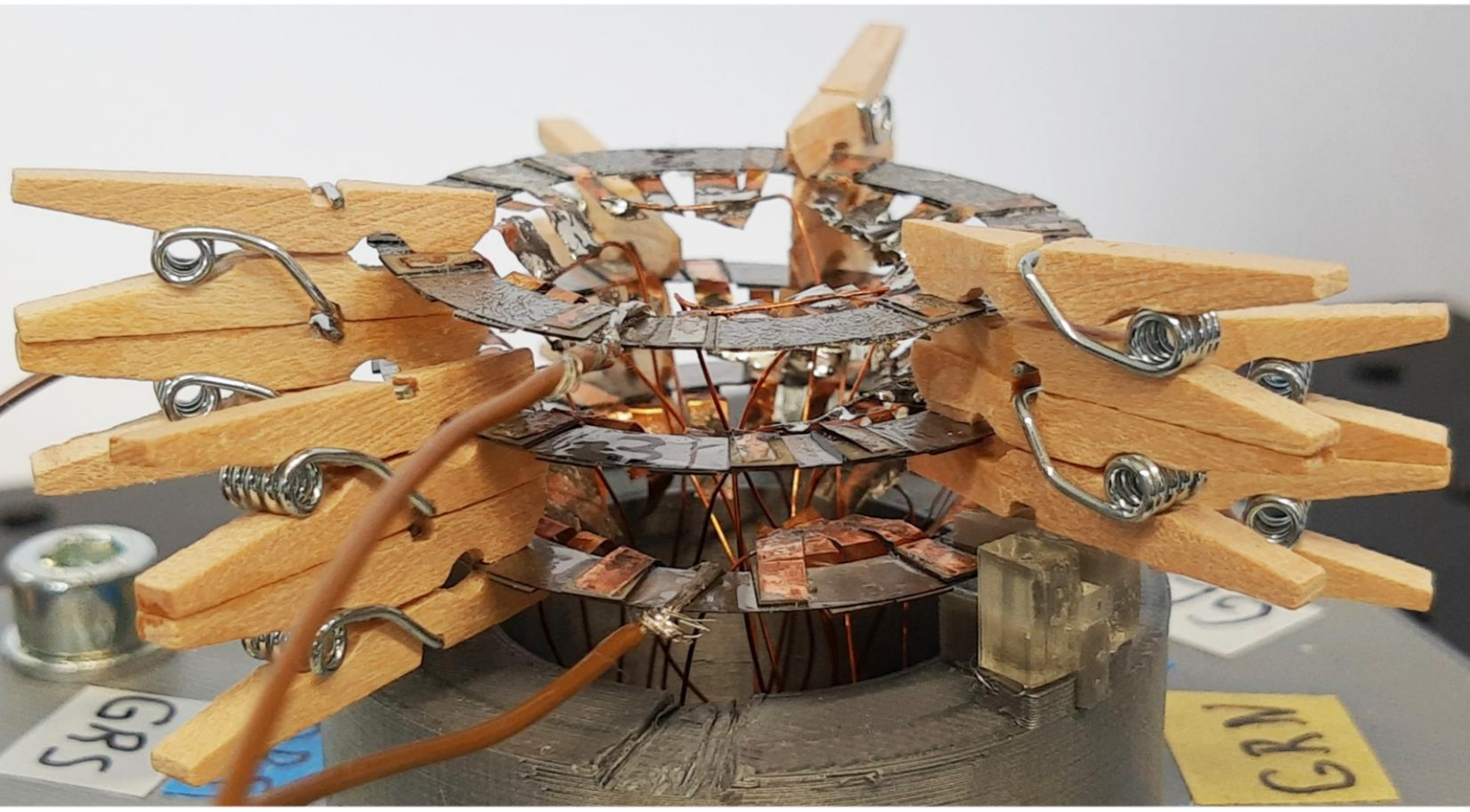

Planar approach for designing and fabricating active metamaterials

By

K. de Jong

in partial fulfilment of the requirements for the degree of

Master of Science
in Mechanical Engineering

at the Delft University of Technology,
to be defended publicly on Wednesday August 31, 2022 at 03:30 PM.

Thesis committee:	Dr. A. Hunt,	TU Delft, Supervisor, Chair
	Dr. N. Bhattacharya,	TU Delft
	Dr S.H. Hossein Nia Kani	TU Delft

TU Delft

Abstract

Shape changing active metamaterial could form the structural backbone of an object as well as deliver the actuation. The integration of these two functions saves design space and allows for creative topologies. The literature study of this thesis investigated smart material actuator solutions that could be used to enable such active metamaterials, covering PVDF, dielectric elastomers, IPMC, conducting polymer, carbon nanotubes and piezoelectric ceramics. It is found that dielectric elastomers achieve high strains, low stress and need high driving voltages. Conducting polymers are able to deliver both high stress and high strain, but consume relatively much power. If power consumption is a priority, Electronic EAPs are preferred. PVDF does not excel on stress or strain, but is an overall good performer. The outlook of realizing active metamaterials via integration of actuation paves the way for non-rigid body deformations and broadens the view on potential applications. At the moment such a system cannot be realized due to the lack of appropriate designs and manufacturing methods. The objectives of this report are (1) the employment of smart materials to make metamaterials active, (2) proposing a method of how to realize this using production materials and (3) employing these methods to build a small metamaterial demonstrator that functions both as the actuator and the structure. In this work this was done by designing and constructing a tube shaped metamaterial demonstrator of a high precision positioning system. The 3D geometry of the metamaterial was built by layering planar pre-fabricated structures which use smart material for actuation. The design of the unit cells can be implemented in metamaterial of any shape and allows for miniaturization, which extends its applicability. The metamaterial was capable of vertical displacements. The constructed metamaterial tube was able to bend itself. Measured maximum amplitudes of a single layer, and the three layered stack were respectively 4.60 µm and 6.91 µm. Roll movement of the top layer of the stack was achieved with a lowest point of -0.13 µm and a highest point of 8.49 µm. The system showed that smart materials are a suitable choice to make metamaterial active, and that active metamaterial could be produced using production material. The planar approach for design and fabrication, provides a relatively simple and fast method for building metamaterial in general.

Contents

1 Introduction

Metamaterials are engineered materials that can attain properties that are very exotic or cannot be attained with natural or classical materials. A well-known metamaterial is the pentamode material that is designed by Milton and Cherkaev [1]. It is a pentamode material that behaves like a fluid. This means that it is easy to deform and hard to compress. For this reason these kind of materials are also called meta-fluids. Metamaterials can be designed in a way to provide characteristics that cannot be found ordinary materials, for example, a re-entrant honeycomb that has a negative poisons ratio [2]. When pulled in vertical direction, instead of getting thinner in horizontal direction, it widens. Negative stiffness is another characteristic that can be achieved by metamaterial, for example by buckling when pushed over a certain boundary [3].

High precision positioning systems are a valuable asset in the race for smaller feature sizes in high tech industry. The power transmission systems of these systems occupy design space which limits the miniaturization of the system. Geared power transmission systems suffer from backlash, which is a fundamental issue that originates from the use of gears. It can be introduced intentionally in the design, but also caused by errors or wear and is the cause of non-linear behavior in the equations of motion of a system [4]. Research on this problem has been done by modelling [4], eliminating this backlash mechanically [5] and compensation it by control [6]. Another complication of the use of gears is the production of wear particles. The mechanical contact between gears can be the reason for the presence of these particles that are caused by fatigue wear, abrasive wear or adhesive wear [7].

If metamaterial would be able to actively change the characteristics and shape of its unit cells, the dimensions of the material could be altered. Unit cells of active metamaterial could form the structural backbone of the object, as well as deliver the actuation. Integrating these two functions in the unit cells would safe valuable design space. As each unit cell could be altered, the object would be able to deform freely. The use of solid state actuators for activation the unit cells could rule out any backlash in actuation. Being able to locally adjust the material, would also allow for the correction of local deformations and isolation of vibrations by the structure itself. These capabilities would extend the potential applicability of shape changing-metamaterial far from positioning systems only. Very few work has been done on actively changing the dimensions of metamaterial by deforming the unit cells. In 2016 a kirimigami inspired study has been done by Overvelde *et al.* which achieved a metamaterial with a tunable shape [8]. The actuators that were used for this study were tactical placed air pockets by which the cubic unit cell could be flattened. In 2021 Navin Shankar Saravana Jothis manufactured shape changing metamaterial with miniaturizable unit cells that were able to amplify the input of piezoelectric actuators by 9.28 times [9]. Work on changing the characteristics of metamaterial actively has been done on stiffness and damping [10].

Smart materials are an interesting option for activating metamaterials. They are material level transducers that convert energy between multiple physical domains, for example from the electrical to the mechanical domain [11]. The transducers can be used for actuating, as well as sensing purposes [6]. Due to their robust [12] and compact build, they do not limit the miniaturizability of the metamaterial. A literature review on electromechanical smart material transducers was conducted to (1) gain the knowledge that is critical for understanding the working principles of the transducers and (2) discover the potential for integrating smart material transducers in the unit cells of metamaterial. The review gathers the characteristics of PVDF, dielectric elastomers, IPMC, conducting polymer, carbon nanotubes and piezoelectric ceramics. Strain, Young's modulus, stress, driving voltage, power consumption and the requirements on their surroundings were reviewed to categorize the materials and composites. It is found that dielectric elastomers achieve high strains, low stress and need high driving voltages. Conducting polymers are able to deliver both high stress and high strain, but consume relatively much power. If power consumption is a priority, Electronic EAPs are preferred. PVDF does not excel on stress or strain, but is an overall good performer.

The use of piezoelectric material in a bending setup to planarly manufacture active metamaterial, was not part of earlier research and has the potential to be miniaturized. At the moment such a system cannot be realized due to the lack of appropriate designs and manufacturing methods. The objectives of this report are

(1) the employment of smart materials to make metamaterials active, (2) proposing a method of how to realize this using production materials and (3) employing these methods to build a small metamaterial demonstrator that functions both as the actuator and the structure. In this work this was done by designing and constructing a tube shaped metamaterial demonstrator of a high precision positioning system. The 3D geometry of the metamaterial was built by layering planar pre-fabricated structures which use smart material for actuation. The design of the unit cells can be implemented in metamaterial of any shape and allows for miniaturization, which extends its applicability. The metamaterial will be validated in measurements on vertical displacements of the individual layers, and measurements on the vertical displacement and roll movement of the stack.

2 A review of electromechanical smart material transducers for planar metamaterial design

The literature review on electromechanical smart material transducers was conducted to (1) gain the knowledge that is critical for understanding the working principles of the transducers and (2) discover the potential for integrating smart material transducers in the unit cells of metamaterial. The review gathers the characteristics of PVDF, dielectric elastomers, IPMC, conducting polymer, carbon nanotubes and piezoelectric ceramics. Strain, Young's modulus, stress, driving voltage, power consumption and the requirements on their surroundings were reviewed to categorize the materials and composites. It is found that dielectric elastomers achieve high strains, low stress and need high driving voltages. Conducting polymers are able to deliver both high stress and high strain, but consume relatively much power. If power consumption is a priority, Electronic EAPs are preferred. PVDF does not excel on stress or strain, but is an overall good performer.

A review of electromechanical smart material transducers for planar metamaterial design

Kees de Jong

***Abstract*—Smart material transducers have a wide area of potential applications such as vibration damping, high precision positioning and sensing. The competitive advantage of smart material transducers is their solid state behaviour. In addition to the absence of backlash due to this solid state, smart material transducers have great miniaturization and integration potentials. This literature study gathers the characteristics of PVDF, dielectric elastomers, IPMC, conducting polymer, carbon nanotubes and piezoelectric ceramics. These materials or composites are potentially suited to be used as foundation for electromechanical activation of planar mechanical metamaterial. To support deliberate actuator choices, Strain, Young's Modulus, Stress, Driving voltage, Power consumption and requirements on their surroundings are reviewed for the aforementioned materials and composites. It is found that dielectric elastomers achieve high strains, low stress and need high driving voltages. Conducting polymers are able to deliver both high stress and high strain, but consume relatively much power. If power consumption is a priority, Electronic EAPs are preferred. PVDF does not excel on stress or strain, but is an overall good performer.**

I. Introduction

Smart material transducers are material level transducers that convert energy between multiple physical domains, for example from the electrical to the mechanical domain [1]. They are compact, robust [2] and easy to manufacture [1] and suffer no backlash due to their solid state behaviour. A variety of materials that can be used for the production of smart material transducers is able to respond very fast to stimuli, which makes them eligible for high bandwidth applications [1]. Smart material transducers can be used for actuating as well as sensing purposes [3].

The combination of these characteristics makes smart material transducers a logical choice for implementation in mechatronics and paves the way for further miniaturization and integration. Smart material transducers are often used for vibration damping due to their fast response. Their simple and compact build makes them suitable for the integration in motion amplifiers. Amplified they deliver sufficient displacement while maintaining high precision which makes them an appropriate choice for high precision positioning systems.

This literature study gathers the characteristics of PVDF, dielectric elastomers, IPMC, conducting polymer, carbon nanotubes and piezoelectric ceramics in section II. These materials or composites are potentially suited to be used as foundation for smart material transducers. The characteristics covered are strain, Young's modulus, stress, driving voltages, power consumption and the requirements on their surroundings. These characteristics are important for the practical application and are discussed in section III.

II. Smart materials for transducers

Two types of smart transducers materials that are frequently used are electro active polymers and piezoelectric ceramics. The polymers that are adressed in this section are divided between electronic and ionic electro active polymers.

A. Electro Active Polymers

Polymers are pliable and relatively inexpensive. Some of them possess the ability to change their shape or size when an electrical, chemical, pneumatic, optical or magnetic field is applied. The most practical excitation for mechatronical applications of these polymers is electrical. These polymers are known as Electro Active Polymers (EAPs), they are mechanically flexible, have a low density and are easy to process [4]. In the early 1990s, EAPs able to induce large strain were introduced [5]. The working principles of EAPs can be categorised by two mechanisms: electronic EAPs which are driven by electric field and ionic EAPs which are driven by the displacement of ions [6].

1) Electronic: The dimensional changes in electronic (field activated) EAPs are caused by piezoelectric, electrostriction and Maxwell stress effects [6]. Electronic EAPs are subdivided by the principal that is their dominant cause for electrostriction. Piezoelectric polymers are characterized by an electrical polarization that can be modified by an applied electric field that applies a moment to the polarized groups within the polymer and physically deforms the the material [4]. Dielectric elastomers deform due to electrostatic interaction between two electrodes with opposite electric charge [7].

Piezoelectric polymers are polar polymers that are almost all in the semicrystaline form [6]. Piezoelectric polymers are ferroelectric when their polarization can be re-orientated by the application of an electric field [6]. This re-orientation of the polarization can produce a contraction in the direction of the applied electric field of up to 5% [6]. Multiple ferroelectric polymers are used to produce actuators such as polyvinyl fluoride (PVF), polyvinylidene fluoride (PVDF, also abbreviated as PVF_2) or copolymers of PVDF with trifluoroethylene (TrFE) or tetrafluoroethylene (TFE). To increase the dielectric constant of the material, electron radiation can be used, but this treatment is known to have several undesirable side effects [8]. A higher electromechanical response with respect to electron radiated material, was realised by the use of

molecular designed terpolymers [4]. The dielectric constant of terpolymers can be increased by using filler with a high dielectric constant [6]. Ferroelectric polymer actuators can also be constructed from two components, a flexible backbone and a grafted polarizable polymer [9][10]. PVDF-based ferroelectic polymers are known to be processed relatively easy and to have large and fast mechanical responses [11]. Driving voltages of manufactured PVDF-based actuators range from $10\,\mathrm{V}$ up to $>1000\,\mathrm{V}$ [12], power consumption is in the range of miliwatts [5] and the Young's modulus is $1462\,\mathrm{MPa}$[13].

The normal ferroelectric transition can be modified by a random defect field to realize a reversible phase transformation between the polar and non-polar molecular forms that converts a normal ferroelectric polymer into a relaxor ferroelectric polymer [14]. Relaxor ferroelectric polymers distinguish themselves from other polymers by their high dielectric constant ($K > 50$) [15] and have a slimmer hysteresis loop compared to normal ferroelectric materials [16]. Figure 1 shows the differences in the polarization hysteresis loops of P(VDF-TrFE) 50/50 copolymer measured at room temperature, before and after irradiation [16].

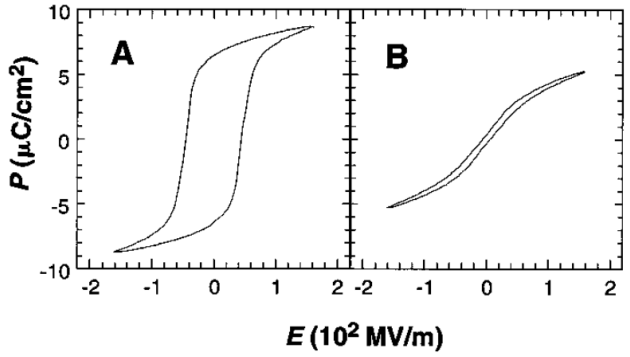

Fig. 1. The polarization hysteresis loops of P(VDF-TrFE) 50/50 copolymer measured at room temperature: (A) before irradiation and (B) after irradiation with 4×10^5 Gy at $120\,^{\circ}\mathrm{C}$ [16].

Dielectric elastomers are actuated by placing a charge on the surfaces of a thin rubbery dielectric. This can be done by spraying the charge on the material [17], but also, more practical, by using compliant electrodes attached to the material [18]. Typical materials that are used to produce dielectric elastomer actuators are polydimethylsiloxane (PDMS) and a pressure sensitive tape fabricated by 3M™[19]. The Young's moduli of these materials lie around $0.5\,\mathrm{MPa}$ [19].

Dielectric elastomers are known to achieve strains greater than 100% [4][5][7]. The process of an expanding dielectric elastomer is shown in Figure 2.

Electromechanical instability can occur within dielectric elastomers due to wrinkling or dielectric breakdown. Studies have shown that this problem can be eliminated by lateral prestretch [20] [21]. Very high bond acrylic tapes (VHB) were commonly used for dielectric material, but suffer from high viscoelasticity which prevents fast response of the actuator. VHB is recently being replaced by silicone-based elastomers

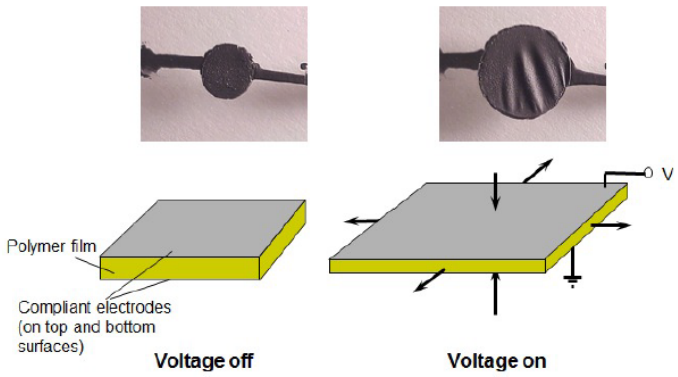

Fig. 2. Photographed and schematic expanding dielectric elastomers [18].

(polysiloxanes) which show lower viscoelasticity, but also low dielectric constants [22].

Broad application of dielectric elastomers is forestalled by the need for relatively high driving voltages in to order of $1\,\mathrm{kV}$ for electrode separetions of 10 to $100\,\mu\mathrm{m}$[23]. Several methods to lower the driving voltage such as decreasing the elastic modulus [24], increasing the dielectric permittivity [25], decreasing the film thickness [26] and chemical modification of polar elastomers [27] are being studied.

Common materials that are used for electrodes on dielectric elastomer actuators include graphite and carbon black. Alternative methods such as compliant metal thin-films, metal-polymer nano-composites and nanoparticle implantation are used to miniaturize dielectric elastomer actuators [28].

2) Ionic: The displacements and shape changes of ionic EAP actuators are caused by the movement of ions through the actuator material. Ionic EAP actuators are manufactured using ionic polymers, conductive electrodes such as metals, conducting polymers and carbon nanotubes. Driving voltages of ionic EAP actuators are in the range of $1\,\mathrm{V}$ to $7\,\mathrm{V}$ and powerconsumption is in the range of milliwatts [5].

IPMCs consists of an ion-exchange polymer film that is coated with metal electrodes. They offer typical strains of 0.5% and a typcial stress of $3\,\mathrm{MPa}$ when exposed to a relatively low driving voltage of $<10\,\mathrm{V}$. Processing IPMCs is relatively easy and their potential for miniaturization is good [29][30]. IPMCs are fabricated by coating an ion-exchanging membrane (IEM) with an electrode material such as metals (e.g., Au, Pt, Pd, Ag) or transition metals (e.g., Ni, Fe) on Nafion films [31]. The Nafion film is soaked in water and when exposed to an electrical field, cations carry water molecules to the cathode side. Hereby the cathode side will expand, while the opposite site will shrink. This causes a bending deformation in the actuator [29]. An illustration of the process is shown in Figure 3. The Young's modulus of manufactured IPMCs varies between $220\,\mathrm{MPa}$ and $830\,\mathrm{MPa}$ [32].

Conventional IPMCs are needed to be submerged in water to operate, but when the water is replaced by an ionic liquid, it is possible for IPMCs to operate in air [33].

Conducting polymer EAPs can be constructed from two or three layers. Bilayer devices are made out of a conductive

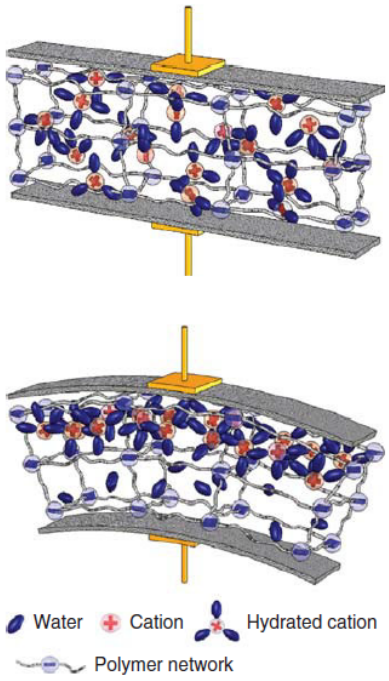

Fig. 3. Schematic illustration of an IPMC structure without an applied field (above) and with an applied field (below). Adapted from [29].

polymer film which acts as an electrode and is connected to a 'no volume-change film'. To make a bilayered device work, a counter-electrode must be present and the device must function in an electrolyte solution [6]. Trilayer devices are constructed from two conducting polymer electrodes with an electrolyte in between to form a bending EAP actuator. A trilayered device functions in an electrolytic solution as well to make ionic conductivity between the two conductive polymer electrodes feasible, a counter-electrode is then not necessary because it is integrated in the actuator. The use of an electrolytic solution can be avoided by using a polymer electrolyte or an ionic polymer gel between the two conducting polymer layers which will act simultaneously as a no volume-change layer [6]. The volume changes that occur in conducting polymer EAPs are caused by the incorporation and expulsion of ions and solvents into, and from the polymer electrodes [34]. Conductive polymer EAPs are known to theoretically be able to produce high force densities up to $450\,\mathrm{MPa}$[35]. Volume changes between oxidized and reduced states are 30-40% [36]. Young's moduli of the actuator depend on the saturation of the material. In 1997 Della Santa *et al.* reported a saturated Young's modulus of $(1450 \pm 76)\,\mathrm{MPa}$ for a linear actuator while the dry Young's modulus was $(2990 \pm 94)\,\mathrm{MPa}$[37].

The main disadvantage of conductive polymer EAPs is that the response time of the actuator is limited by the ion exchange process between the conductive polymer film and the electrolytic medium. The response time is typically in the order of seconds [38]. The most efficient way to improve this ion exchange process is to increase the ionic conductivity of the electrolytic medium. This could be done by increasing the ion concentration when a liquid electrolyte is used but thereby the actuator is forced to work in a liquid medium [6].

Carbon nanotube EAPs expand when charge is stored in the nanotubes. Strains of up to 0.6% are reported [39]. The arrangement of individual nanotubes has proven difficult to control [40]. The Young's modulus of carbon nanotubes is very high and known to be a function of the tube radius and helicity. In general it is in the range of $1\,\mathrm{TPa}$ [41].

The working principle of ionic EAPs is a flow of ions which is a disadvantage when power consumption is considered. The current that is needed for actuation has to be maintained to keep the actuator in actuated position.

B. Ceramics

Piezoelectric ceramics are ferroelectric materials in which the ferroelectric behavior is not observed above a certain temperature called the Curie temperature (T_C) [42].

Ceramics are the most widely used materials for the production of piezoelectric smart material transducers. The most commonly used ceramic is lead zirconate titanate [43] which was introduced in the 1960s [44] and is abbreviated as PZT. Unlike electro active polymers, ceramic based smart material transducers are inflexible and brittle. Ceramic based stacked smart materials generally produce relatively small strain, large stress and have a low respone time [1]. Larger strains are obtained by bending actuators based on ceramics and composites such as macrofiber composites (MFCs).

The toxicity of lead-based transducers has led to the discovery of lead free alternatives based on $Na_{0.5}Bi_{0.5}TiO_3$ (NBT) and $K_{0.5}Na_{0.5}NbO_3$ (KNN) showing challenging characteristics such as a strong temperature depence and degradation [45].

1) PZT: PZT is a polycrystalline ceramic material that is the most commonly used option for the production of ceramic actuators. The material consist of a solid solution of ferroelectric lead titanate ($PbTiO_3$) and an anti-ferroelectric lead zirconate ($PbZr_3$). The crystalline structure of PZT can be altered by changing the ratio of the two components in the material. For solutions with relatively much titanate, the material is tetragonal. Relatively high amounts of zirconate produce rhombohedral material. Coexistance of both phases is also possible whereby 14 different polarization directions are achievable [46]. Structural changes of PZT at Curie temperature and morphotropic phase boundary are shown in Figure 4.

Due to the application of an electric field, the titanate or zicronate ion moves along the direction of the applied field, which causes the deformation of the actuator.

The properties of PZT can be influenced by the addition of isovalent, donor or acceptor dopants. These dopants can influence the piezo properties, curie point, permittivity, cation vacancy, electromechanical coupling factor k_p, mechanical quality factor Q_m, dielectric loss and create anion vacancies [47]. Typical strains are in the order of 0.1% [48] and typical Young's moduli are in the range of $85\,\mathrm{GPa}$ [49]. Thin films

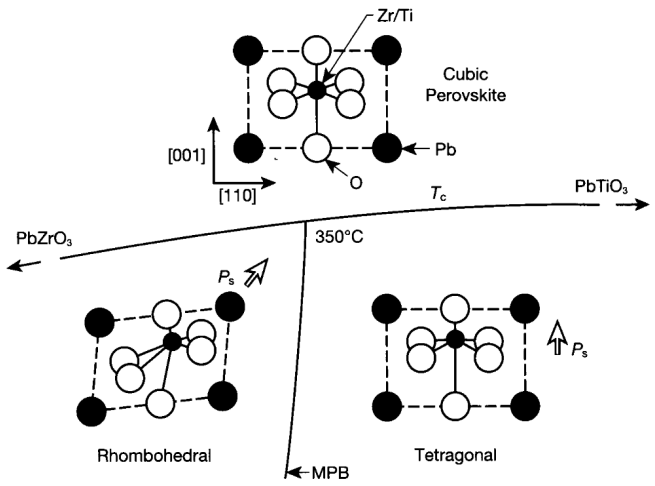

Fig. 4. Portion of the PZT phase diagram showing structure changes at Curie temperature and morphotropic phase boundary [46].

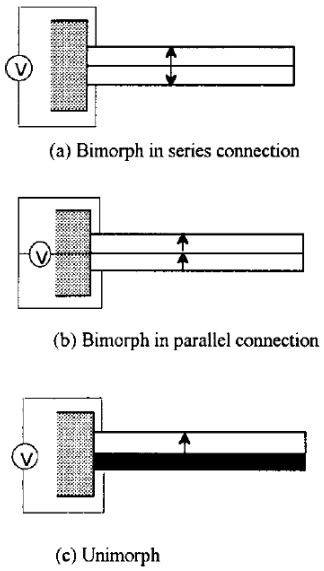

Fig. 5. Piezoelectric bimorph series (a), parrallel (b) and unimorph (c) actuators adapted from [56].

of PZT with largely detached columnar grains showed strains of 0.9% [50]. Driving voltages for PZT actuators are in the range of $2.5\,\mathrm{V}$ to $600\,\mathrm{V}$, mainly depending on the thickness of the actuator [51] [52] [53] [54].

To multiply the stroke of a PZT actuator, PZT- and electrode layers can be placed in an alternate manner upon each other to form a multilayered stack. Thick layered stacks that need to be driven by higher fields (due to thickness of the stack) can be fabricated by cutting pre-sintered blocks and electroding, poling and bonding them. Thinner stacks that require lower driving voltages can be fabricated by a tape casting technique where very thin tapes are produced and stacked on top of each other. The displacement of multilayered PZT stacks is generally around $1\,\mu\mathrm{m}$ / $1\,\mathrm{mm}$ of height [47]. To achieve more practical displacements, actuator stacks are generally placed within an amplifying mechanism.

2) Ceramic Bending actuators: To enlarge the low strain that is delivered by the piezoelectric ceramic material, the material can be placed in a bending configuration. The most common bending actuator configurations are unimorph and bimorph actuators [55]. Unimorph actuators consist of one piezoelectric layer and one flexible layer that is not piezoelectric. When a field is applied to the piezoelectric layer, the dimensions of this layer will change. The neutral layer will resist these changes and thereby the actuator is forced to bend. Bimporh actuators consist of two piezoelectric layers which, dependant on a parallel or series electrical connection, are respectively poled in the same or opposite direction [55]. The different assemblies of bi- and unimorph actuators are shown in Figure 5.

3) Piezoceramic fibers: Aforementioned restrictions of piezoceramic actuators such as brittleness and small displacements can also be remedied by using piezoceramic material in a polymeric matrix [57]. The strenght of crystalline materials is usually much higher in fiber form and the flexible nature of the polymer matrix makes the actuator bendable. The interdigitated electrodes that are visible in Figure 6 causes much higher forces/displacements due to the stronger longitudinal (d_{33}) piezoelectric effect [58]. These composites are available under multiple commercial titles such, Active Fiber Composite (AFC) and Macro Fiber Composites (MFC).

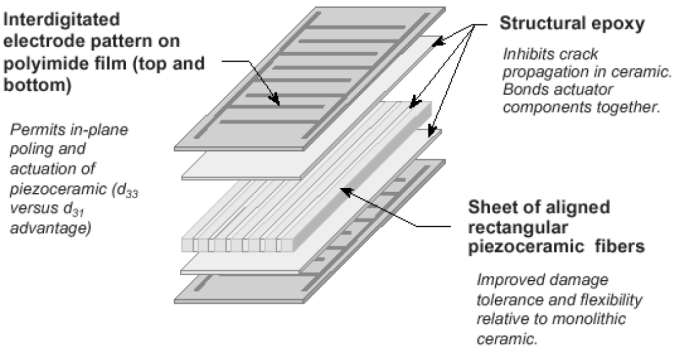

Fig. 6. A schematic view of MFC adapted from [58].

Piezoceramic fiber for the use in actuators such as AFC actuators were traditionally extruded in a cylindrical form which made the manufacturing process, and thereby the actuators, expensive. MFC was developed by the NASA Langley Research Center by using low-cost piezoceramic wafers that were diced to produce the needed fibers. The costs of producing and handling the fibers became much lower by this manufacturing technique [57]. As is visible in Figure 6, the piezoceramic fibers wihtin MFC are rectangular shaped due to the dicing and surrounded by a polymer matrix. Maximum operational strain rates of 0.099% and operational stress rates of $33\,\mathrm{MPa}$ at driving voltages of $3\,\mathrm{kV}$ are reported in literature [57] for LaRC-MFC™baseline actuators. Like normal

piezoceramic actuators, piezoceramic fiber actuators have no special requirements on their surroundings. Comprehensive information about manufacturing techniques and applications of several piezoceramic fiber actuators including AFC and MFC can be found in an overview written by Williams in 2002 [58].

III. Discussion

In section II the characteristics of EAPs, ceramics and SMAs were discussed. The performance of these materials as the foundation of a smart material transducer depends on their behavior in the fields of strain, stress, driving voltage, response, power consumption and requirements on their surroundings. These aspects of the different materials described in section II is summarized in Table I. Stresses are estimated by multiplying the strain with the Young's modulus as can be seen in Equation 1.

$$\sigma = \varepsilon E \tag{1}$$

In section II it was found that, next to differences in stress and strain, the materials distinguish themselves on driving voltages, power consumption and whether or not there is a need for an electrolytic surrounding. While all ionic actuators fundamentally have the need for an electrolytic surrounding, literature presents several ways of how this surrounding can be omitted [6] [33]. The choice for a material to form an actuator should be made on the specific demands of the application. As can be seen in Table I, there is no material without disadvantages. If power consumption is not an issue for the specific application, conducting polymers are closest to an adequate all-rounder.

IV. Conclusion

The eligibility of the different materials for the use in smart material transducers depends on demands of the end-user.

- High strains are achieved by dielectric elastomer actuators at the downside that they produce relatively few stress and need very high driving voltages.
- Carbon nanotube actuators are able to produce very high stress but are difficult to manufacture. Conducting polymer actuators are able to deliver high stress and strain. A drawback to carbon nanotube actuators, conducting polymer actuators and fundamentally all ionic EAP actuators is that they consume large amounts of power.
- Electronic EAP actuators are preferred if there is a need for low power consumption. An alternative that consumes slightly more power could be provided by ceramic actuators.
- Ionic EAP actuators are able to function on low driving voltages. They do however, have the need for an electrolytic environment. While this environment can be achieved in several more or less intrusive ways, it complicates the manufacturing process of both actuator and instrument.
- PVDF based actuators do not excel on stress nor strain, but are overall good achievers with practical stress and strain values. They functions on driving voltages starting at $10\,\mathrm{V}$, consume little power and have no restrictions on their surroundings.

Nomenclature

K	Dielectric constant [–]
k_p	Electromechanical Coupling Factor [–]
Q_m	Mechanical Quality Factor [–]
E	Young's modulus [Pa]
σ	Stress [Pa]
ε	Strain [–]
P	Polarization [$\mathrm{C\,m^{-2}}$]
E	Electric field [$\mathrm{V\,m^{-1}}$]
T_C	Curie temperature [°C]

References

[1] D. J. Leo, *Engineering analysis of smart material systems*. Wiley Online Library, 2007, vol. 435.

[2] P. Jänker and W. Martin, *Performance and characteristics of actuator materials*. Deutsche Aerospace AG (DASA), 1993.

[3] A. Hunt, Z. Chen, X. Tan, and M. Kruusmaa, "An integrated electroactive polymer sensor–actuator: design, model-based control, and performance characterization," *Smart Materials and Structures*, vol. 25, no. 3, p. 035016, 2016.

[4] Y. Bar-Cohen and I. A. Anderson, "Electroactive polymer (eap) actuators—background review," *Mechanics of Soft Materials*, vol. 1, no. 1, pp. 1–14, 2019.

[5] J.-H. Bae and S.-H. Chang, "Pvdf-based ferroelectric polymers and dielectric elastomers for sensor and actuator applications: a review," *Functional Composites and Structures*, vol. 1, no. 1, p. 012003, 2019.

[6] Y. Bar-Cohen, *Electroactive polymer (EAP) actuators as artificial muscles: reality, potential, and challenges*. SPIE press, 2004, vol. 136.

[7] A. O'Halloran, F. O'malley, and P. McHugh, "A review on dielectric elastomer actuators, technology, applications, and challenges," *Journal of Applied Physics*, vol. 104, no. 7, p. 9, 2008.

[8] P.-Y. Mabboux and K. K. Gleason, "19f nmr characterization of electron beam irradiated vinylidene fluoride–trifluoroethylene copolymers," *Journal of Fluorine Chemistry*, vol. 113, no. 1, pp. 27–35, 2002.

[9] J. Su, J. Harrison, T. S. Clair, Y. Bar-Cohen, and S. Leary, "Electrostrictive grafr elastomers and applications," *MRS Online Proceedings Library (OPL)*, vol. 600, 1999.

[10] J. Su, J. S. Harrison, and T. L. S. Clair, "Electrostrictive graft elastomers," Feb. 4 2003, uS Patent 6,515,077.

[11] S. T. Choi, J. O. Kwon, and F. Bauer, "Multilayered relaxor ferroelectric polymer actuators for low-voltage operation fabricated with an adhesion-mediated film transfer technique," *Sensors and Actuators A: Physical*, vol. 203, pp. 282–290, 2013. [Online]. Available: https://www.sciencedirect.com/science/article/pii/S0924424713004330

[12] P. Martins, D. Correia, V. Correia, and S. Lanceros-Mendez, "Polymer-based actuators: back to the future," *Physical Chemistry Chemical Physics*, vol. 22, no. 27, pp. 15 163–15 182, 2020.

[13] M. El Achaby, F. Arrakhiz, S. Vaudreuil, E. Essassi, and A. Qaiss, "Piezoelectric β-polymorph formation and properties enhancement in graphene oxide–pvdf nanocomposite films," *Applied Surface Science*, vol. 258, no. 19, pp. 7668–7677, 2012.

[14] Q. Chen, K. Ren, B. Chu, Y. Liu, Q. Zhang, V. Bobnar, and A. Levstik, "Relaxor ferroelectric polymers–fundamentals and applications," *Ferroelectrics*, vol. 354, pp. 178–191, 08 2007.

[15] M. R. Gadinski, Q. Li, G. Zhang, X. Zhang, and Q. Wang, "Understanding of relaxor ferroelectric behavior of poly (vinylidene fluoride–trifluoroethylene–chlorotrifluoroethylene) terpolymers," *Macromolecules*, vol. 48, no. 8, pp. 2731–2739, 2015.

[16] Q. Zhang, V. Bharti, and X. Zhao, "Giant electrostriction and relaxor ferroelectric behavior in electron-irradiated poly (vinylidene fluoride-trifluoroethylene) copolymer," *Science*, vol. 280, no. 5372, pp. 2101–2104, 1998.

TABLE I
COMPARISON OF ACTUATOR MATERIALS

	EAP elect. PVDF	**EAP elect. Dielect. elast.**	**EAP ionic IPMC**	**EAP ionic Conduct. pol.**	**EAP ionic Carbon nano.**	**Ceramics**	**Piezocer. fibers**
Strain	5%	100%	0.5%	30%-40%	0.60%	0.1%	0.099%
Young's Modulus [MPa]	1462	0.5	220 - 830	1450 (saturated)	$1e6$	$85e3$	$3.33e4$
Stress [MPa]	73.1	0.5	1.1 - 4.15	435 - 580	6000	85	33
Driving voltage [V]	10-1200	>1000	<10	1-7	1-7	2.5-600	3000
Power consumption	++	++	–	–	–	++	++
Surroundings	Boundless	Boundless	Electrolytic	Electrolytic	Electrolytic	Boundless	Boundless

[17] C. Keplinger, M. Kaltenbrunner, N. Arnold, and S. Bauer, "Röntgen's electrode-free elastomer actuators without electromechanical pull-in instability," *Proceedings of the National Academy of Sciences*, vol. 107, no. 10, pp. 4505–4510, 2010.

[18] R. Pelrine, Q. Pei, and R. Kornbluh, "Dielectric elastomers: past, present, and potential future," in *Electroactive Polymer Actuators and Devices (EAPAD) XX*, vol. 10594. International Society for Optics and Photonics, 2018, p. 1059406.

[19] P. Sommer-Larsen and A. L. Larsen, "Materials for dielectric elastomer actuators," in *Smart Structures and Materials 2004: Electroactive Polymer Actuators and Devices (EAPAD)*, vol. 5385. International Society for Optics and Photonics, 2004, pp. 68–77.

[20] S. J. A. Koh, T. Li, J. Zhou, X. Zhao, W. Hong, J. Zhu, and Z. Suo, "Mechanisms of large actuation strain in dielectric elastomers," *Journal of Polymer Science Part B: Polymer Physics*, vol. 49, no. 7, pp. 504–515, 2011.

[21] S. J. A. Koh, C. Keplinger, R. Kaltseis, C.-C. Foo, R. Baumgartner, S. Bauer, and Z. Suo, "High-performance electromechanical transduction using laterally-constrained dielectric elastomers part i: Actuation processes," *Journal of the Mechanics and Physics of Solids*, vol. 105, pp. 81–94, 2017.

[22] F. B. Madsen, A. E. Daugaard, S. Hvilsted, and A. L. Skov, "The current state of silicone-based dielectric elastomer transducers," *Macromolecular rapid communications*, vol. 37, no. 5, pp. 378–413, 2016.

[23] F. Carpi, S. Bauer, and D. De Rossi, "Stretching dielectric elastomer performance," *Science*, vol. 330, no. 6012, pp. 1759–1761, 2010.

[24] D. M. Opris, M. Molberg, C. Walder, Y. S. Ko, B. Fischer, and F. A. Nueesch, "New silicone composites for dielectric elastomer actuator applications in competition with acrylic foil," *Advanced Functional Materials*, vol. 21, no. 18, pp. 3531–3539, 2011.

[25] P. Brochu and Q. Pei, "Dielectric elastomers for actuators and artificial muscles," *Electroactivity in polymeric materials*, pp. 1–56, 2012.

[26] A. Poulin, S. Rosset, and H. R. Shea, "Printing low-voltage dielectric elastomer actuators," *Applied Physics Letters*, vol. 107, no. 24, p. 244104, 2015.

[27] D. M. Opris, "Polar elastomers as novel materials for electromechanical actuator applications," *Advanced Materials*, vol. 30, no. 5, p. 1703678, 2018.

[28] S. Rosset and H. R. Shea, "Flexible and stretchable electrodes for dielectric elastomer actuators," *Applied Physics A*, vol. 110, no. 2, pp. 281–307, 2013.

[29] I.-S. Park, K. Jung, D. Kim, S.-M. Kim, and K. J. Kim, "Physical principles of ionic polymer–metal composites as electroactive actuators and sensors," *MRS bulletin*, vol. 33, no. 3, pp. 190–195, 2008.

[30] F. Carpi and E. Smela, *Biomedical applications of electroactive polymer actuators*. John Wiley & Sons, 2009.

[31] L. Raymond, J.-F. Revol, D. Ryan, and R. Marchessault, "Precipitation of ferrites in nafion® membranes," *Journal of applied polymer science*, vol. 59, no. 7, pp. 1073–1086, 1996.

[32] Q. He, M. Yu, L. Song, H. Ding, X. Zhang, and Z. Dai, "Experimental study and model analysis of the performance of ipmc membranes with various thickness," *Journal of Bionic Engineering*, vol. 8, no. 1, pp. 77–85, 2011.

[33] M. D. Bennett and D. J. Leo, "Ionic liquids as stable solvents for ionic polymer transducers," *Sensors and Actuators A: Physical*, vol. 115, no. 1, pp. 79–90, 2004.

[34] K. Okabayashi, F. Goto, K. Abe, and T. Yoshida, "Electrochemical studies of polyaniline and its application," *Synthetic Metals*, vol. 18, no. 1-3, pp. 365–370, 1987.

[35] R. Baughman, "Conducting polymer artificial muscles," *Synthetic metals*, vol. 78, no. 3, pp. 339–353, 1996.

[36] E. Smela and N. Gadegaard, "Surprising volume change in ppy (dbs): an atomic force microscopy study," *Advanced Materials*, vol. 11, no. 11, pp. 953–957, 1999.

[37] A. Della Santa, D. De Rossi, and A. Mazzoldi, "Characterization and modelling of a conducting polymer muscle-like linear actuator," *Smart Materials and Structures*, vol. 6, no. 1, p. 23, 1997.

[38] G. Alici and N. N. Huynh, "Performance quantification of conducting polymer actuators for real applications: a microgripping system," *IEEE/ASME Transactions On Mechatronics*, vol. 12, no. 1, pp. 73–84, 2007.

[39] T. Mirfakhrai, J. Y. Oh, M. Kozlov, S. L. Fang, M. Zhang, R. H. Baughman, and J. D. Madden, "Carbon nanotube yarns as high load actuators and sensors," in *Advances in Science and Technology*, vol. 61. Trans Tech Publ, 2008, pp. 65–74.

[40] R. H. Baughman, A. A. Zakhidov, and W. A. De Heer, "Carbon nanotubes–the route toward applications," *science*, vol. 297, no. 5582, pp. 787–792, 2002.

[41] N. Yao and V. Lordi, "Young's modulus of single-walled carbon nanotubes," *Journal of applied physics*, vol. 84, no. 4, pp. 1939–1943, 1998.

[42] C. Moure and O. Peña, "Recent advances in perovskites: Processing and properties," *Progress in Solid State Chemistry*, vol. 43, no. 4, pp. 123–148, 2015.

[43] H. Jaffe, "Piezoelectric ceramics," *Journal of the American Ceramic Society*, vol. 41, no. 11, pp. 494–498, 1958.

[44]

[45] T. R. Shrout and S. J. Zhang, "Lead-free piezoelectric ceramics: Alternatives for pzt?" *Journal of Electroceramics*, vol. 19, no. 1, pp. 113–126, 2007.

[46] R. E. Newnham, "Molecular mechanisms in smart materials," *MRS Bulletin*, vol. 22, no. 5, pp. 20–34, 1997.

[47] P. Panda and B. Sahoo, "Pzt to lead free piezo ceramics: a review," *Ferroelectrics*, vol. 474, no. 1, pp. 128–143, 2015.

[48] T. Fey, F. Eichhorn, G. Han, K. Ebert, M. Wegener, A. Roosen, K.-i. Kakimoto, and P. Greil, "Mechanical and electrical strain response of a piezoelectric auxetic pzt lattice structure," *Smart Materials and Structures*, vol. 25, no. 1, p. 015017, 2015.

[49] W. Jaffe, "Cook, and h. jaffe, piezoelectric ceramics," 1971.

[50] M. D. Nguyen, E. P. Houwman, and G. Rijnders, "Large piezoelectric strain with ultra-low strain hysteresis in highly c-axis oriented pb (zr 0.52 ti 0.48) o 3 films with columnar growth on amorphous glass substrates," *Scientific reports*, vol. 7, no. 1, pp. 1–9, 2017.

[51] S. Park and S. He, "Standing wave brass-pzt square tubular ultrasonic motor," *Ultrasonics*, vol. 52, no. 7, pp. 880–889, 2012.

[52] P. Muralt, M. Kohli, T. Maeder, A. Kholkin, K. Brooks, N. Setter, and R. Luthier, "Fabrication and characterization of pzt thin-film vibrators for micromotors," *Sensors and Actuators A: Physical*, vol. 48, no. 2, pp. 157–165, 1995.

[53] M. Sitti, D. Campolo, J. Yan, and R. S. Fearing, "Development of pzt and pzn-pt based unimorph actuators for micromechanical flapping mechanisms," in *Proceedings 2001 ICRA. IEEE International Conference on Robotics and Automation (Cat. No. 01CH37164)*, vol. 4. IEEE, 2001, pp. 3839–3846.

[54] M. Koch, A. Evans, and A. Brunnschweiler, "The dynamic micropump driven with a screen printed pzt actuator," *Journal of Micromechanics and Microengineering*, vol. 8, no. 2, p. 119, 1998.

[55] X. Gao, J. Yang, J. Wu, X. Xin, Z. Li, X. Yuan, X. Shen, and S. Dong, "Piezoelectric actuators and motors: materials, designs, and applications," *Advanced Materials Technologies*, vol. 5, no. 1, p. 1900716, 2020.

[56] Q.-M. Wang, Q. Zhang, B. Xu, R. Liu, and L. E. Cross, "Nonlinear piezoelectric behavior of ceramic bending mode actuators under strong electric fields," *Journal of Applied Physics*, vol. 86, no. 6, pp. 3352–3360, 1999.

[57] W. K. Wilkie, R. G. Bryant, J. W. High, R. L. Fox, R. F. Hellbaum, A. Jalink Jr, B. D. Little, and P. H. Mirick, "Low-cost piezocomposite actuator for structural control applications," in *Smart structures and materials 2000: industrial and commercial applications of smart structures technologies*, vol. 3991. International Society for Optics and Photonics, 2000, pp. 323–334.

[58] R. B. Williams, G. Park, D. J. Inman, and W. K. Wilkie, "An overview of composite actuators with piezoceramic fibers," *Proceeding of IMAC XX*, vol. 47, p. 130, 2002.

3 Planar approach for designing and fabricating active metamaterials

Shape changing active metamaterial could form the structural backbone of an object as well as deliver the actuation. The integration of these two functions saves design space and allows for creative topologies. The outlook of realizing active metamaterials via integration of actuation paves the way for non-rigid body deformations and broadens the view on potential applications. At the moment such a system cannot be realized due to the lack of appropriate designs and manufacturing methods. The objectives of this paper are (1) the employment of smart materials to make metamaterials active, (2) proposing a method of how to realize this using production materials and (3) employing these methods to build a small metamaterial demonstrator that functions both as the actuator and the structure. In this work this was done by designing and constructing a tube shaped metamaterial demonstrator of a high precision positioning system. The 3D geometry of the metamaterial was built by layering planer pre-fabricated structures which use smart material for actuation. The design of the unit cells can be implemented in metamaterial of any shape and allows for miniaturization, which extends its applicability. The metamaterial was capable of vertical displacements, and the constructed tube was able to bend itself. The measured maximum amplitudes of a single layer and the three layered stack were respectively 4.60 μm and 6.91 μm. Roll movement of the top layer of the stack was achieved with a lowest point of -0.13 μm and a highest point of 8.49 μm. The system showed that smart materials are a suitable choice to make metamaterial active, and that active metamaterial could be produced using production material. The planar approach for design and fabrication, provides a relatively simple and fast method for building metamaterial in general.

Planar approach for designing and fabricating active metamaterials

Kees de Jong

***Abstract*—Shape changing active metamaterial could form the structural backbone of an object as well as deliver the actuation. The integration of these two functions saves design space and allows for creative topologies. The outlook of realizing active metamaterials via integration of actuation paves the way for non-rigid body deformations and broadens the view on potential applications. At the moment such a system cannot be realized due to the lack of appropriate designs and manufacturing methods. The objectives of this paper are (1) the employment of smart materials to make metamaterials active, (2) proposing a method of how to realize this using production materials and (3) employing these methods to build a small metamaterial demonstrator that functions both as the actuator and the structure. In this work this was done by designing and constructing a tube shaped metamaterial demonstrator of a high precision positioning system. The 3D geometry of the metamaterial was built by layering planar pre-fabricated structures which use smart material for actuation. The design of the unit cells can be implemented in metamaterial of any shape and allows for miniaturization, which extends its applicability. The metamaterial was capable of vertical displacements. The constructed metamaterial tube was able to bend itself. Measured maximum amplitudes of a single layer, and the three layered stack were respectively $4.60\,\mu\mathrm{m}$ and $6.91\,\mu\mathrm{m}$. Roll movement of the top layer of the stack was achieved with a lowest point of $-0.13\,\mu\mathrm{m}$ and a highest point of $8.49\,\mu\mathrm{m}$. The system showed that smart materials are a suitable choice to make metamaterial active, and that active metamaterial could be produced using production material. The planar approach for design and fabrication, provides a relatively simple and fast method for building metamaterial in general.**

I. Introduction

High precision positioning systems are a valuable asset in the race for smaller feature sizes in high tech industry. The power transmission systems of these systems occupy design space which limits the miniaturization of the system. Geared power transmission systems suffer from backlash, which is a fundamental issue that originates from the use of gears. It can be introduced intentionally in the design, but also caused by errors or wear and is the cause of non-linear behavior in the equations of motion of a system [1]. Research has been done on modelling [1], eliminating this backlash mechanically [2] and compensation it by control [3]. Another complication of the use of gears is the production of wear particles. The mechanical contact between gears can be the reason for the presence of these particles that are caused by fatigue wear, abrasive wear or adhesive wear [4].

If metamaterial would be able to actively change the characteristics and shape of its unit cells, the dimensions of the material could be altered. Unit cells of active metamaterial could form the structural backbone of the object, as well as deliver the actuation. Integrating these two functions in the unit cells would safe valuable design space. As each unit cell could be altered, the object would be able to deform freely. The use of solid state actuators for activation the unit cells could rule out any backlash in actuation. Being able to locally adjust the material, would also allow for the correction of local deformations and isolation of vibrations by the structure itself. These capabilities would extend the potential applicability of shape changing-metamaterial far from positioning systems only.

Very few work has been done on actively changing the dimensions of metamaterial by deforming the unit cells. In 2016 a kirimigami inspired study has been done by Overvelde et al. which achieved a metamaterial with a tunable shape [5]. The actuators that were used for this study were tactical placed air pockets by which the cubic unit cell could be flattened. In 2021 Jothis manufactured shape changing metamaterial with miniaturizable unit cells that were able to amplify the input of piezoelectric actuators by 9.28 times [6].

The use of piezoelectric material in a bending setup to planarly manufacture active metamaterial, was not part of earlier research and has the potential to be miniaturized. At the moment such a system cannot be realized due to the lack of appropriate designs and manufacturing methods. The objectives of this report are (1) the employment of smart materials to make metamaterials active, (2) proposing a method of how to realize this using production materials and (3) employing these methods to build a small metamaterial demonstrator that functions both as the actuator and the structure. In this work this was done by designing and constructing a tube shaped metamaterial demonstrator of a high precision positioning system. The 3D geometry of the metamaterial was built by layering planar pre-fabricated structures which use smart material for actuation. The design of the unit cells can be implemented in metamaterial of any shape and allows for miniaturization, which extends its applicability. The metamaterial will be validated in measurements on vertical displacements of the individual layers, and measurements on the vertical displacement and roll movement of the stack.

The remainder of this paper is organized as follows. In section II the methodology for designing, modelling, realizing and testing active metamaterial consisting of three stacked planar rings is outlined. The results of fabrication, as well as the results of measurements on vertical displacement and roll movement, are shown in section III. These results and the opportunities for further research are discussed in section IV

whereafter the conclusion is reached in section V.

II. Methods & materials

In subsection II-A the logic behind the design and the choice of materials is explained. The expected displacement is calculated in subsection II-B. Fabrication and the use of materials are described in subsection II-C whereafter the measurements setups and the conducted experiments are described in subsection II-D.

A. Design

At the moment, additive manufacturing methods are not mature enough to make active metamaterial. An alternative method is to assemble active metamaterial from simple prefabricated components. This can be realized by separately fabricating the active and passive components, and afterwards laminating them. Afterwards the laminated layers can be stacked into a metamaterial.

Active metamaterial is able to locally adjust the stress or strain profile within the material. The use of piezoelectric actuators enables the actuation to be compactly integrated in the metamaterial. This makes a separate motor redundant and saves design space.

In this study this technique is employed to realize a cylindrical demonstrator of such active metamaterial. This design is representative of a range of potential active metamaterial applications, such as an enclosure of a machine, an actuated optical column or a positioning stage.

The choice of using the actuators in a bending setup is made to amplify the range of the actuators. This omits the need for a motion amplifier. The tunability of each unit cell enables the metamaterial to deform freely. Hereby not only vertical displacement can be reached, the tube will also be able to bend itself in a desired direction.

A planar design is chosen because it simplifies manufacturing. The layers can be seen in Figure 1a. Two layers are connected to form the unit cells of the metamaterial. A unit cell is showed in Figure 1b. These cells can be stacked to form the metamaterial and increase the range. The planar design consist of a spring steel ring with six segments that each contain 4 laser cut piezoceramic elements. These elements are aligned in such a way that they create a wave form in the spring steel ring when they contract. The placement of the actuators and the wave form are visible in respectively Figure 1a and Figure 1b. The design of the stacked rings that form the metamaterial is showed in Figure 2. After every two waves, the ring is connected to the ring above. This results in three evenly distributed connections between every ring. Dividing the rings in pairs of two waves was originally intended to provide width compensation when actuating the stack.

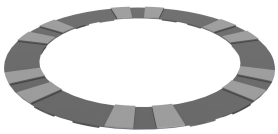

(a) Actuators on the ring.

(b) Wave formed by actuators during actuation.

Fig. 1: Placement of actuators.

Fig. 2: Metamaterial design.

B. Modelling

The concept that is used to create displacement is the concept of a unimorph actuator. Such an actuator is simply a contracting piece of material bonded to a flexible sub layer. The expected displacement δ for an actuator like this, is calculated by equations for unimorph actuators [7] [8] clamped at one side and can be seen in Equation 1.

$$\begin{aligned} \delta &= \frac{3l^2}{h_p^2}\frac{AB(B+1)}{D}d_{31}V \\ A &= \frac{E_s}{E_p} \\ B &= \frac{h_s}{h_p} \\ D &= A^2B^4 + 2A(2B + 3B^2 + 2B^3) + 1 \end{aligned} \tag{1}$$

PZT-5H and 1.4310 stainless steel properties as well as actuator length can be found in Table I. For the sake of simplicity the calculations are done for a rectangle actuator. The outcome of Equation 1 is a displacement of $3.13\,\mu\mathrm{m}$.

Young's modulus PZT-5H	E_p [Pa]	61*10^9
Young's modulus 1.4310 stainless steel	E_s [Pa]	193*10^9
Density PZT-5H	ρ_p [$\mathrm{kg\,m^{-3}}$]	7500
Density 1.4310 stainless steel	ρ_s [$\mathrm{kg\,m^{-3}}$]	7872
Coupling factor	d_{31} [$\mathrm{C\,N^{-1}}$]	320*10^-12
Voltage	V	80
Height PZT-5H	h_p [m]	0.19*10^-3
Height 1.4310 stainless steel	h_s [m]	0.10*10^-3
Length of the actuaor	l [m]	3.0-10^-3

TABLE I: Material properties.

The placement of two actuators close together in a scheme as is visible in Figure 1b should give double this displacement which is $6.26\,\mu\mathrm{m}$.

C. Realisation

The actuators for this project that are visible in Figure 1a should have a shape that follows the form of the flexible ring that is underneath. Therefor a plate material was preferred that would allow for cutting it into the right shape. PZT-5H Piezoelectric Plate (PSI-5H4E) was chosen as actuator material because of its availability in plates and that it is easily cuttable by laser. The rated drive voltages are +/-84 V. The material expands in thickness direction and contracts in length and width direction if an electric field of the same polarity and orientation as the original polarization field is applied. Motion in thickness direction of the plate with a thickness of $0.19\,\mathrm{mm}$ is in the order of tens of nanometers. Motion in length direction of the plate with a length of $34.9\,\mathrm{mm}$ is in the order of microns [9]. Cutting PZT in the desired shape will be done using and Optec WS STARTER laser micro machining system which uses a Talon 355-12 (15 W) laser.

The ring beneath the actuators visible in Figure 1a is the flexible sub layer of the design. For this layer, $0.1\,\mathrm{mm}$ 1.4310 stainless steel is chosen because it is flexible, conductive, durable and suitable to multiple adhesion techniques such as welding and glueing. Cutting the spring steel in the desired shape will be done using the same Optec laser as is used for cutting the PZT.

Multiple assembling techniques were used during the realisation of the metamaterial. To fixate the PZT elements on the spring steel ring, an alignment and clamping tool was designed. The model of this clamping tool is shown in Figure 3. The clamping tool will be printed on a Formlabs Form 3+ stereolithography printer. The bottom layer will be printed using Formlabs Grey V4 resin. It has three columns distributed evenly at the outside of the design to align the second and third layer. The part will function as an inlay for PZT elements and secures room for spacers between the rings. It accommodates 24 PZT elements of each 11 degrees and 12 spacers of each 5 degrees. The margins between each element or spacer are 1 degree. The spacers will connect the individual layers to form the metamaterial. The peaks of the bottom layer will be connected to the valleys of the upper layer. This way will allow for the displacements of the individual rings to add up. The spacers will be placed between the waved layers at three points distributed evenly over the six waves in the ring. The middle layer will be made from Formlabs Elastic 50A to ensure sufficient flexibility. It is intended to put equal pressure on the ring and has a flat surface with three small blocks of material placed at the outer diameter of the ring. These blocks can fixate the ring and center it. The flexibility of the part will compensate for minor imperfections when the setup is pressurized. The top layer functions as a force distributor which distributes the force of the clamp evenly to the flexible middle layer. The top layer will be made from the same material as the bottom layer to provide the needed stiffness.

To prevent exposure of the glue to excessive amounts of heat, the PZT elements will be soldered before they are glued.

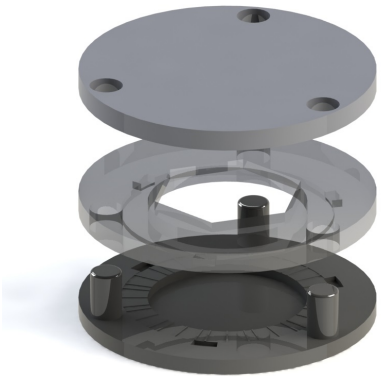

Fig. 3: Clamping tool.

To keep the elements flat, they will be soldered onto copper foil. The flatness is needed to fit them in the alignment tool after soldering. Soldering will be done using low temperature Chipquik SMD291SNL (Sn96.5/Ag3.0/Cu0.5) soldering paste. Strips of copper foil will be laid down on a hot plate. A drip of soldering paste will be placed on the strip, after which the PZT element will be placed upon the drip. When subsequently the hot plate is turned on, the elements will be soldered to the copper strips.

The actuators will be glued to the spring steel ring. This ring will replace the function of the electrode to which it is glued. Glueing the actuators onto the spring steel will be done with slow hardening, two component, epoxy glue. The slow hardening characteristics of this glue provides 30 minutes handling time which will be welcome while aligning the actuators. Due to clamping during the glueing period, the layer thickness of the glue will be very thin compared to the thickness of the PZT. Both combinations will act as parallel plate capacitors. The characteristics of the new parallel plate capacitor that is slightly thicker by the added layer of glue, should not change significantly compared to the original one. The added layers can be seen in Figure 4.

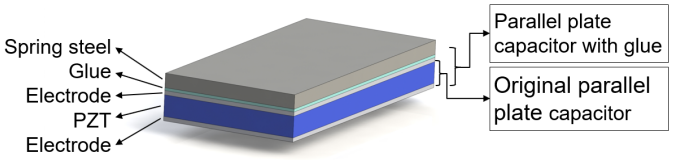

Fig. 4: Original and new parallel plate capacitor with glue.

The copper strips connected to the PZT elements will be wired by soldering coated $0.25\,\mathrm{mm}$ copper wire onto strips. The elements will be wired per group of 4 PZT elements which together form a wave. The spring steel ring, which functions as the negative electrode, will be wired by winding a wire around the ring and afterwards soldering the winding. Although the solder will not bond to the stainless steel, this process will result in mechanical friction between the wire and the ring.

The first layer will be fixed on 3D printed base by using printed clamps. Stacking the second layer on the first layer, as well as stacking the third layer on the second layer, will be done using non permanent fasteners. These fasteners will fixate the layers with respect to each other and provide spacing between the layers. They distribute the displacement of the bottom layer to the one above. By using this non definitive connection between the layers, the formed metamaterial remains detachable. Choosing the placement of the fasteners will be done by finding three approximately equal displacements on the bottom ring and connecting those to three valleys of the top ring. This process is discussed later in this section and in section IV.

D. Experiments

During the experiments the amplitudes and displacements of segments are measured when a signal is fed to one, multiple, or all of the segments of a ring or a stack. The measurements were focused on vertical displacement and measurements on width compensation were omitted. Recommendations for further research on this matter can be read in subsection IV-B. Roll movement will be achieved by choosing specific segments in each layer to become active. These segments will be chosen based on their relative position towards the fastener that is wished to distribute the displacement to the next layer.

Two measurement setups were used during the experiments. A single point setup for fast measurements in a single point, and a multipoint setup to measure the deformation of an entire layer. The setups present the movement of the metamaterial in a different way. The single point setup shows displacement, where the multipoint setup shows the amplitude of an oscillation.

1) Single point: Single point measurements for displacement were done on a setup consisting of a National Instruments NI USB-6211 multifunction I/O device and a laptop running Labview software to generate functions and read the inputs from the Micro-Epsilon ILD1750-2 laser distance sensor. This sensor uses optical triangulation to define the distance of an object relative to the sensor. The setup can be seen in Figure 5. The generated singal was amplified by an Smart Materials MFc 1500/20 high voltage amplifier. The output of these measurements are the voltage on the system, the measured displacement, and the current through the system at every $0.01\,\mathrm{s}$. The results were analysed using Matlab. The signals that were fed to the metamaterial are two sines of $1\,\mathrm{Hz}$. One between $0\,\mathrm{V}$ and $76.2\,\mathrm{V}$, and one between $-84\,\mathrm{V}$ and $84\,\mathrm{V}$.

2) Multipoints: Multipoint measurements were done by a Polytec PSV-400 scanning laser Doppler vibrometer (LDV) setup visible in Figure 6. A laser is pointed at a moving target, the reflected beam has Doppler shift due to the motion of the target. The vibrometer can be set to do these measurements on multiple points. Displacements are calculated from this data by the accompanying software. Multiple measurement points are presented in an image laid over a picture of the object to give a 3D visualization. The signals that were fed to the metamaterial are two sines of $1\,\mathrm{Hz}$ with relatively $V_{min} = 0\,\mathrm{V}$ & $V_{top} = 80\,\mathrm{V}$ and $V_{min} = -84\,\mathrm{V}$ & $V_{top} = 84\,\mathrm{V}$. These signals were generated by the vibrometer controller and amplified by a Thorlabs HV200 amplifier. Results were analysed using the following settings: point data, single scan point and displacement that was calculated from velocity.

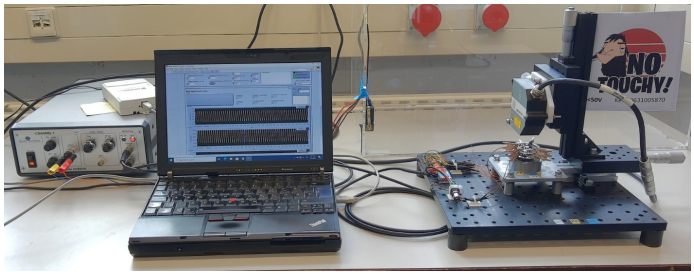

Fig. 5: Single point setup.

Fig. 6: Multipoint setup.

The signal was kept above $0\,\mathrm{V}$ and below $84\,\mathrm{V}$ during the bulk of the experiments. The choice to keep the voltage positive at first, was made due to concerns of depolarization. After consulting the manufacturer, negative voltages were used in the last stage of the experiments. $84\,\mathrm{V}$ was the maximum rated voltage for the PZT plates by the manufacturer. The current through an actuator can be calculated by Equation 2 [10].

$$\begin{aligned} i &= C\frac{\partial u(t)}{\partial t} \\ u(t) &= A\sin\omega t \\ i(t) &= CA\omega\cos\omega t \end{aligned} \tag{2}$$

Where the capacitance C of the used actuator is $80\,\mathrm{nF}$ [9] which results in a current with an amplitude of $10^{-6}\mathrm{A}$ for the used frequencies and voltages. Currents this small are not measurable by the used setups.

III. Results

The results are divided into the results of the fabrication process in subsection III-A and the results of the measurements in subsection III-B.

A. Fabrication

Laser cutting the spring steel resulted in a flat ring with an outer diameter of $40\,\mathrm{mm}$ and an inner diamter of $30\,\mathrm{mm}$ without any bends or scratches which was desired for later processing. The cut ring is showed in Figure 7.

Fig. 7: Laser cut spring steel.

The pzt plates were cut into segments of a ring with the same dimensions as the spring steel ring. Mutiple of this segments cut from a PZT plate are shown in Figure 8.

Fig. 8: Laser cut PZT plate.

The design of the clamping tool as was described in section II, results in an evenly filled out bottom layer of the tool visible in Figure 9.

The result of soldering the PZT elements to copper strips using a hot plate can be seen in Figure 10. The achieved, flatness which is needed to fit them in the alignment tool, is shown in Figure 9. The result of the PZT elements glued upon the spring steel ring is shown in Figure 11. Winding a wire around the ring and afterwards soldering the wire results in a low resistance of around $1\,\Omega$ from the wire to the ring.

The clamps that are used to fix the first layer on the base can be seen in Figure 12. Stacking the second layer on the first layer, as well as stacking the third layer on the second layer, was done by using two adjusted miniaturized clothespins glued together. The stacks of two and three layers are showed in respectively Figure 13a and Figure 13b. The segments that are activated to achieve roll are visible in Table III and correspond to the positions shown in Figure 14. The abbreviations are based on the accompanying wire colors in Dutch and are written out in Table II.

B. Measurements

1) Individual rings: The maximum amplitudes of the rings with all segments active were measured to analyse the following subjects:

Fig. 9: PZT elements with copper foil in inlay.

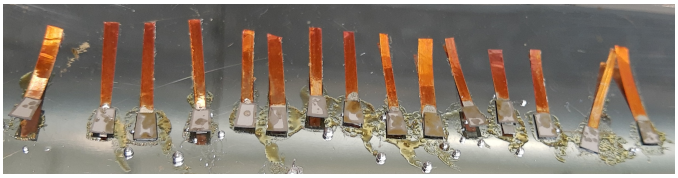

Fig. 10: Several PZT elements soldered onto copper foil.

- The performance of the individual rings
- The variation between the rings
- The influences of the clamps
- The influence of the segments on each other

The results for measuring the maximum amplitudes of ring 1, 2 and 3 with all six segments active are shown in respectively Figure 15a, Figure 15b and Figure 15c. These experiments achieved maximum amplitudes in the range of $3.9\,\mu\mathrm{m}$ to $4.6\,\mu\mathrm{m}$. Zero displacement is shown at the 3 places where the rings are clamped to the base. Large variations in segment performance is shown in all rings. For ring 1, segment WT shows the lowest amplitude, for ring 2, segment WT shows the lowest amplitude and for ring 3, segment GRS shows the lowest amplitude. Minimum and maximum amplitudes of each of the three rings are shown in Table IV.

To get to know the influence that the combinations of segments have on each other, the three combinations of segments between the clamping points are activated. The results for measuring the amplitudes of the combinations of ring 2 are shown in Figure A.6, Figure A.7 and Figure A.8. Comparable amplitudes in the range of $3.28\,\mu\mathrm{m}$ up to $3.94\,\mu\mathrm{m}$ are measured.

The variations between the segment of a single ring were studied by measuring the amplitudes of the individual segments of ring 3. The results of these measurements are shown

Fig. 11: Prototype ring with PZT elements.

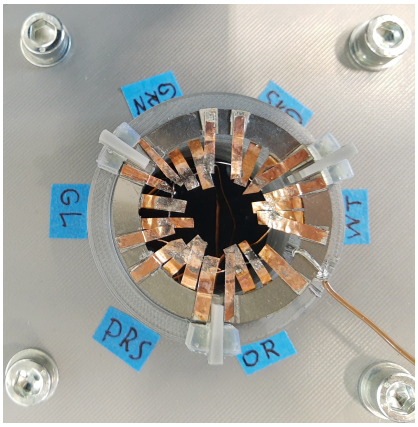

Fig. 12: First layer clamped on base.

in Figure A.9 up to Figure A.14. The maximum amplitude of each segment of ring 3 is shown in Table V.

To compare the measurements of the single point setup with the multipoint setup, the displacement and amplitude of segment GL is measured by both setups. The results of these measurements are visible in Figure A.2 and Figure 15a. The maximum displacement and amplitude are shown in Table VI.

2) Stacking the rings: To find three approximately equal displaced segments to interconnect by the improvised clamps, measurements on the amplitudes of the bottom layers were done. The results of these measurements are shown in Figure A.15 up to Figure A.17. After stacking the middle layer on the bottom layer, the amplitude distribution of the displacement by the improvised clamps is checked. Ideally these measurements should show comparable results to the first measurements. To check this distribution, the connection points of the clothespins on the middle layer are measured. These connection points are the valleys of the middle layer. The results of these measurements are shown in Figure A.18 up to Figure A.20. A summary of the measurements is given in Table VII. These measurements are repeated on the middle layer to find attachment points for the top layer. The results of these measurements are shown in Figure A.21 up to Figure A.23. The results of the measurements on the connection points of the top layer are shown in Figure A.24 up to Figure A.26. A summery of the measurements is given in Table VIII.

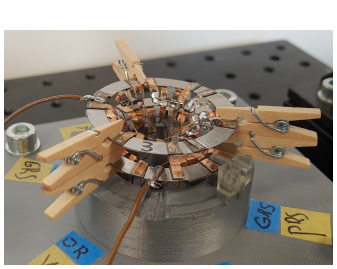

(a) Two layered stacked metamaterial.

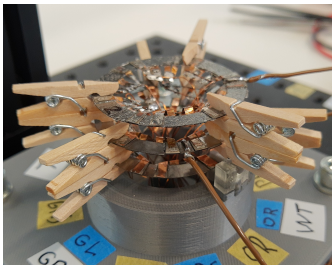

(b) Three layered stacked metamaterial.

Fig. 13: Stacked metamaterial.

Orange	OR
White	WT
Gray	GRS
Green	GRN
Yellow	GL
Purple	PRS

TABLE II: Wire color abbreviations

Stacking the layers to add up the displacements and increase the range of the metamaterial is an important goal of this study. The displacement and the amplitude of segments GRS and PRS were measured by respectively the single point setup and the multipoint setup. To see the effect of stacking the layers, measurements were done on all segments. The results of these measurements are showed in Figure A.2 and Figure 16a. A comparison of the measurements is given in Table IX.

Bending is on of the expected features of the presented metamaterial concept. For this bending action, roll movement of the top of the stack is needed. This movement was experimentally checked by activating the segments shown in Table III from section III. To see the effect of activating these segments, measurements on all segments were done during roll movement. The results of these measurements can be seen in Figure 16b. The lowest point shows an amplitude of $-0.13\,\mu\text{m}$ while the highest point is showing an amplitude of $8.49\,\mu\text{m}$.

To increase the range of motion, the actuation was extended to the maximum allowed range. The displacement and amplitude of segment WT were measured, while feeding a signal of $V_{min} = -84\,\text{V}$ and $V_{max} = 84\,\text{V}$. The results of these measurements on displacement and amplitude can be seen in respectively Figure A.2 and Figure 16c. A comparison between the measurements is given in Table X. To compare the response of the system while being fed a positive signal, to the response while being fed a both positive and negative signal, a measurement on the system without input is needed. The result of this measurement, together with measurements for the plus and plus-minus signals, using the single point setup is shown in Figure A.1. The measurement stated approximately $9.8\,\mu\text{m}$.

IV. Discussion

A. Discussion

1) Measurements and expected displacement: The expected outcome of the design is that only positive displacements

Top	GRN	GRS	WT
Middle	GRS	WT	OR
Bottom	GL	PRS	OR

TABLE III: Active segments for roll.

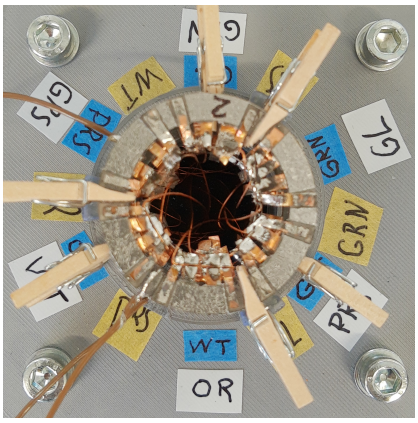

Fig. 14: Top view of the stack with annotated segments (Bottom: blue, middle: yellow, top: white).

should occur when positive voltages are applied. When both positive and negative voltages are applied, also negative displacements should be visible. This expectation is validated by measurements on the single point setup with a zero volt singal, a strictly positive signal and a both positive and negative signal. The results of these measurements are shown in Figure A.1. It can be seen that measurements with only positive voltages do not show values below the 'zero measurement'. The measurement with both positive and negative values shows comparable amplitudes up and under the 'zero measurement'.

The multipoint setup is a vibrometer that is intended to show vibrations. While only positive voltages are applied and only positive displacements occur, the software 'wants' to show a vibration which results in a measurement with an amplitude that is half of the actual value and a movement that goes both 'up' and 'down'. Valley to peak values of the multipoint setup are comparable to the single point setup. This can be seen in Figure 16c where the same signal was fed to the system as the Plus-Minus signal in Figure A.1. For the sake of simplicity, amplitude measurements of the multipoint setup were not converted.

2) Individual rings: The concept of multiple actuators on the top and bottom of a ring was able to successfully create waves in a ring. Thereby the concept can be used to create vertical displacements and could be interesting for building positioning systems. In section II an expected displacement of $6.26\,\mu\mathrm{m}$ was noted. The equation that is used, is for an actuator that is clamped at one side, and moving freely at the other. Table VI shows displacements of around $8\,\mu\mathrm{m}$ which is in the same range. Differences between the calculated value and the measured value are likely to occur due to influences of clamping, other segments and alignment faults which result in more or less space between actuators then was intended.

There are variations in the amplitudes of the segments of

	Ring 1	**Ring 2**	**Ring 3**
Min. ampl. [µm]	0.543	1.133	0.057
Max. ampl. [µm]	3.939	4.148	4.600

TABLE IV: Results for actuating all segments for ring 1, 2 and 3. Minimum and maximum segment amplitudes are given for each individual ring.

	GL	**GRN**	**GRS**	**OR**	**PRS**	**WT**
Max. displ. [µm]	2.92	3.61	2.59	1.55	1.53	2.87

TABLE V: Results for actuating all segments for ring 3. Amplitudes are given for each individual segment.

ring 1, which is visible in Figure 15a. One cause that likely contributes to these variations is the misalignment of the actuators of segment WT. The actuators moved slightly during the glueing process which resulted in overlap of the top and bottom actuators, as well as rotations. These misalignments are notable if looked closely at in Figure 15a. Variations in the amplitudes of ring 2 and 3 are believed to be the result of clamping the rings on to the base. This effect is better visible in Figure A.6 where the ring seems to pivot around the lowest clamping point.

Table V shows variations in the amplitudes of the individual segments of ring 3. Segments OR and PRS show less amplitude when compared to the other segments. In Figure A.12 and Figure A.13 it can be seen that the surrounding segments of both segment OR and PRS are 'pushed' below zero. The reason for this behavior could be a variation in clamping force of the lowest clamping point when compared to the other two clamping points, as the behavior is not showed around other clamping points in Figure A.9 up to Figure A.14.

3) Stacking the rings: Three rings were successfully stacked into a metamaterial which resulted in an increased range. The created metamaterial can both function as the structural backbone of a system as well as the actuation part. Stacks of the unit cells can be formed in any wished shape which extends the applicability of the concept. Next to the ability to create a vertical displacement, the metamaterial also proved capable of creating roll movement. This allows the metamaterial tube to bend itself in every wished way. Due to the miniaturizability of the concept, the bending of the tube could be interesting for applications other than positioning such as application in the medical field.

Measurements done on segments GRS and PRS of the top layer of the three layered stack were shown in Table IX. Amplitudes and displacements of the stack proved to be larger than amplitudes and displacements of the individual rings.

Table VII and Table VIII show differences between the amplitudes of the attachment points of the clothespins on the lowest ring, and the amplitudes of the clothespins connected to the highest ring. These differences are visible for both the connections between the bottom ring and the middle ring, as well as for the connection between the middle ring and the top ring. The differences are both positive and negative. The highest measured difference in amplitude is $1.77\,\mu\mathrm{m}$ for

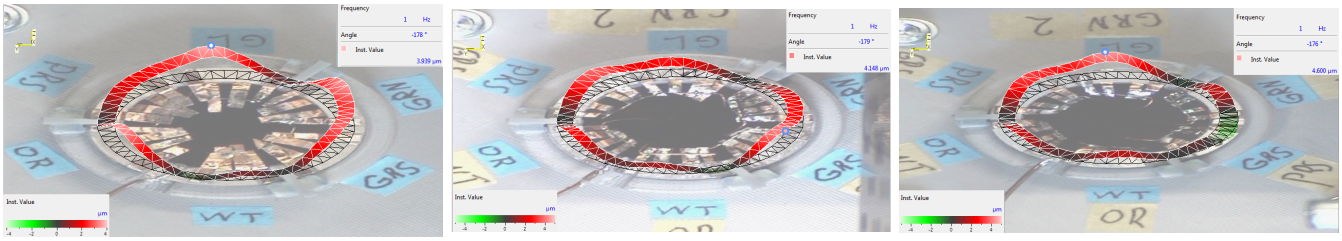

(a) Ring 1 (b) Ring 2 (c) Ring 3

Fig. 15: Results for measurements on maximum amplitudes of ring 1, 2 and 3 with all six segments active.

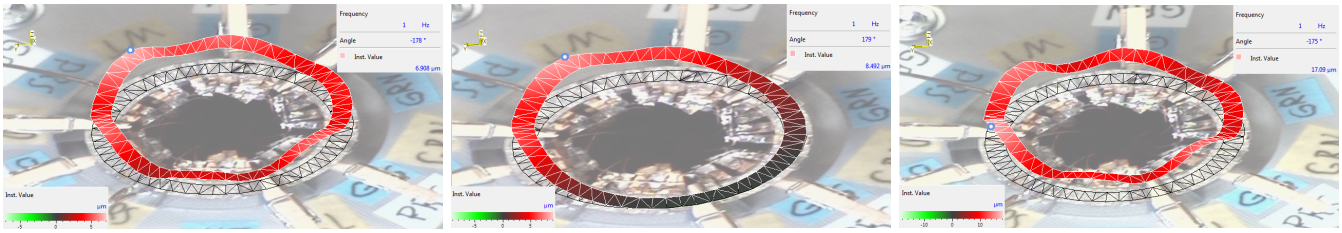

(a) Measurement on segment GRS with all segmetns active.

(b) Measurement on segment PRS during roll movement.

(c) Stack, three layers, WT, $V_{min} = -84\,\mathrm{V}$ and $V_{max} = 84\,\mathrm{V}$.

Fig. 16: Results for measurements on the three layered stack.

	Ring 1 GL
Multi (amplitude) [µm]	3.94
Single (displacement) [µm]	≈ 8

TABLE VI: Results for measurements on segment GL of ring 1 with both multipoint and single point setup.

	GL	**GRS**	**OR**
Peak [µm]	2.98	1.68	1.90
Valley [µm]	2.33	0.89	2.89

TABLE VII: Results for measurements on peaks of bottom ring and corresponding valleys of middle ring.

	OR	**GRS**	**GL**
Peak [µm]	4.05	4.13	3.79
Valley [µm]	3.50	3.27	2.02

TABLE VIII: Results for measurements on peaks of middle ring and corresponding valleys of top ring.

	GRS	**PRS**
Multi [µm]	6.91	5.62
Single [µm]	≈ 12.5	≈ 12.5

TABLE IX: Results of actuating all segments of the stack. Amplitudes and displacements of segment GRS and PRS are given.

segment OR between the middle and the top ring. A possible explanation of these relatively large differences can be found in the stiffness of the wires that were used to drive the actuators. By choosing thin coated copper wires, the stiffness of the wiring was minimalized during design. It was however found that $0.1\,\mathrm{mm}$ stainless steel rings, in combination with the actuators, does not provide large stiffness. While guiding the wires of the middle and top ring through the bottom ring, the stack showed movement. Despite minimalizing the tension on the wires after installing the middle and top layer, there could be some tension left that resulted in displacements within the stack. Considering the low weight of the layers, the weight of the added layer is not expected to contribute to the differences.

Roll movement showed a relatively large maximum amplitude of $8.49\,\mu\mathrm{m}$ from segment GRS. This value is larger than the value of $6.91\,\mu\mathrm{m}$ that was measured at the same point with all the segments of the three layered stack active. An explanation for this behavior could be that tension is build up by the activation of some segments which counteracts the intended motion.

Driving the stack with a sine signal between $-84\,\mathrm{V}$ and $84\,\mathrm{V}$, more than doubled the measured displacement compared to driving the stack with a sine signal which was kept between $0\,\mathrm{V}$ and $84\,\mathrm{V}$. This can be seen in Figure A.1 where the results are showed for measurements with the single point setup, without setting the minimum displacement to zero. This figure also shows the result of approximately $9.8\,\mu\mathrm{m}$ for a measurement without input. When the both positive and negative signal is fed to the system, Figure A.1 shows that this point can be viewed as the middle point around which the system oscillates. The lowest value is approximately $-8\,\mu\mathrm{m}$, the highest $28\,\mu\mathrm{m}$.

4) Metamaterial: The results that were presented in section III showed that the proposed methodology proved suited for building active metamaterial. The relatively simple fabrication process is suitable for miniaturization and allows for up scaling the production of metamaterial. These characteristics make active metamaterial more accessible and broaden the employability, which paves the way for further research on

	Stack WT
Multi (amplitude) [µm]	17.09
Single (displacement) [µm]	≈ 36

TABLE X: Results of actuating all segments of the stack. Amplitudes and displacements of segment WT are given. $V_{min} = -84\,\mathrm{V}$ and $V_{max} = 84\,\mathrm{V}$.

metamaterial structures.

B. Further research

The methodology that is presented allows for a relatively simple and fast production process of active metamaterial. This makes active metamaterial a more competitive option in many research problems and should lead to more implementations in designs. To encourage this, the planar design of active metamaterial should be further investigated and combined with control.

The locally tunable unit cells of active metamaterials could be ideal for absorbing high local impacts such as bullets. Planarly designing such a device could keep costs low and fabrication relatively simple. A controller could manage the collaboration off all unit cells to gradually absorb the energy and safely distribute it to the human body. The unit cell for such a project should be able to change its shape, stiffness and damping rapidly. Smart material actuators could provide the fast response that is needed to achieve this.

For future work on this particular design, it would be interesting to further study the characteristics of the metamaterial. For example, the tunability of the shape of the unit cells can be exploited to create a material with tuneable damping and stiffness when it would be complemented with control. This project focused only on displacements of the active metamaterial setup. The layers are made up out of flexible material and the actuators are suitable for high bandwidth applications. This combination would make it interesting to study the dynamical behavior. The metamaterial proved very capable of roll movement as was discussed earlier in this section. It would be interesting to build a controller to control the movement of the material and study the performance on this matter.

Improvements on the metamaterial can be made by changing the design for a specific goal, optimizing the alignment and clamping tool, the use of thicker spring steel and refinement of the spacers. The design with six waves and three connection points was originally intended to provide width compensation when actuating the stack. To make this possible, a new rest state of 50% actuation was proposed as can be seen in Figure 17a. Vertical enlargement of the stack would not cause a narrower stack as the neighbor segment would compensate for the narrowing. This process is showed in the fully actuated state in Figure 17b. During the experiments, measurements were focused on vertical displacement of the stack and measurements on width were omitted. Experiments on width compensation with the demo model could provide useful information for applications where the width should

(a) 50% actuated stack. (b) 100% actuated stack.

Fig. 17: Width compensation.

remain unchanged. Driving the stack with a controller instead of manually, would highly simplify this experiment.

If the aforementioned width compensation is not pursued, three waves would suffice per layer. This would allow for more room per actuator on the ring. Hereby not only tip displacement δ can be exploited, but also the rotation angle of the tip in combination with the space between the actuators. This way, with less actuators, a larger displacement can be achieved.

Further development of the alignment and clamping tool could provide more consistent placement of the actuators on the stainless steel rings. This would rule out a large amount of the uncertainties faced while interpreting the results. If the actuators are capable of bending thicker stainless steel rings, these rings could provide more stiffness to the setup. A demonstrator which deformations are visible with the naked eye could be designed by choosing different actuator material and pair it with a matching flexible sublayer. A higher stiffness of the setup would result in a relatively lower influence of the stiffness of the wires on the setup. Ideally the clamping points on the base should be as thin as possible. This way they will take up the least amount of torque, which will minimize the influence on the behavior of the ring. The adjusted clothespins that are used, are clamped on the rings. This provides a sufficient connection for low frequency use. If dynamical behavior would be of interest, a more rigid connection between the rings would be preferred.

V. Conclusion

The objectives of this study were (1) the employment of smart materials to make metamaterials active, (2) proposing a method of how to realize this using production materials and (3) employing these methods to build a small metamaterial demonstrator that functions both as the actuator and the structure. This work designed and constructed a tube shaped metamaterial demonstrator of a high precision positioning system. The system showed that smart materials are a suitable choice to make metamaterial active, and that active metamaterial could be produced using production material. The

planar approach for design and fabrication provides a relatively simple and fast method for building metamaterial in general. The metamaterial was capable of vertical displacements, and the constructed tube was able to bend itself. The measured maximum amplitudes of a single layer and the three layered stack were respectively $4.60\,\mu\mathrm{m}$ and $6.91\,\mu\mathrm{m}$. Roll movement of the top layer of the stack was achieved with a lowest point of $-0.13\,\mu\mathrm{m}$ and a highest point of $8.49\,\mu\mathrm{m}$. The metamaterial that was created can both function as the structure of a system, as well as provide the actuation. The methodology that is presented allows for a relatively simple and fast production process of active metamaterial. This makes active metamaterial a more competitive option in many research problems and should lead to more implementations in designs. To encourage this, the planar design of active metamaterial should be further investigated and combined with control. The locally tunable unit cells of active metamaterials could be ideal for absorbing high local impacts such as bullets. Smart material actuators could provide the fast response that is needed to achieve this. For future work on this particular design, it would be interesting to further study the characteristics of the metamaterial. For example, the tunability of the shape of the unit cells can be exploited to create a material with tuneable damping and stiffness when it would be complemented with control.

REFERENCES

[1] S. THEODOSSIADES and S. NATSIAVAS, "Non-linear dynamics of gear-pair systems with periodic stiffness and backlash," *Journal of Sound and vibration*, vol. 229, no. 2, pp. 287–310, 2000.

[2] R. Slatter and R. Degen, "Miniature zero-backlash gears and actuators for precision positioning applications," in *Proc. of 11th European Space Mechanisms and Tribology Symposium ESMATS*, 2005, pp. 9–16.

[3] W. Huang, L. Cai, and X. Tang, "Adaptive repetitive output feedback control for friction and backlash compensation of a positioning table," in *Proceedings of the 37th IEEE Conference on Decision and Control (Cat. No. 98CH36171)*, vol. 2. IEEE, 1998, pp. 1250–1251.

[4] G. P. Stachowiak, G. W. Stachowiak, and P. Podsiadlo, "Automated classification of wear particles based on their surface texture and shape features," *Tribology International*, vol. 41, no. 1, pp. 34–43, 2008.

[5] J. T. Overvelde, T. A. De Jong, Y. Shevchenko, S. A. Becerra, G. M. Whitesides, J. C. Weaver, C. Hoberman, and K. Bertoldi, "A three-dimensional actuated origami-inspired transformable metamaterial with multiple degrees of freedom," *Nature communications*, vol. 7, no. 1, pp. 1–8, 2016.

[6] N. Jothis, "Active metamaterial unit cells incorporating piezoelectric actuator."

[7] Q.-M. Wang, Q. Zhang, B. Xu, R. Liu, and L. E. Cross, "Nonlinear piezoelectric behavior of ceramic bending mode actuators under strong electric fields," *Journal of Applied Physics*, vol. 86, no. 6, pp. 3352–3360, 1999.

[8] Q.-M. Wang, X.-H. Du, B. Xu, and L. E. Cross, "Electromechanical coupling and output efficiency of piezoelectric bending actuators," *IEEE transactions on ultrasonics, ferroelectrics, and frequency control*, vol. 46, no. 3, pp. 638–646, 1999.

[9] "T107-H5NO-1107 piezoelectric plate," https://support.piezo.com/article/62-material-properties#chips, accessed: 2022-07-26.

[10] "Electrical operation of piezo actuators," https://www.piceramic.com/en/expertise/piezo-technology/properties-piezo-actuators/electrical-operation/, accessed: 2022-08-02.

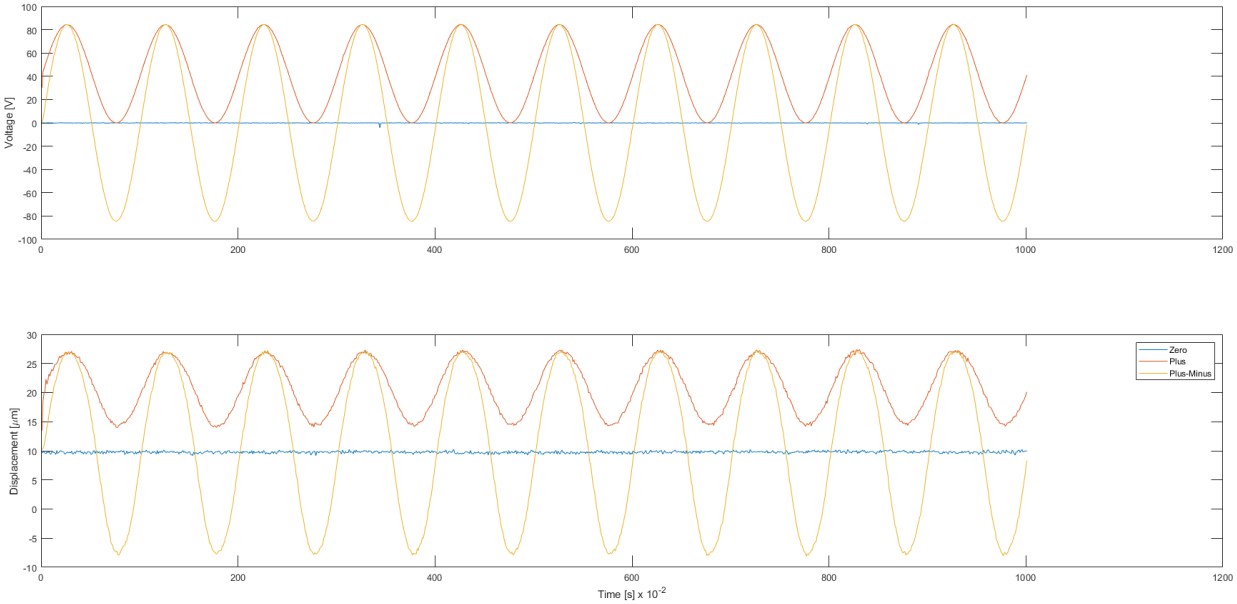

Fig. A.1: Stack 3L WT, single point. ”Zero”: no actuation, ”plus”: 0-84V and ”plus minus”: bipolar -84 to 84V.

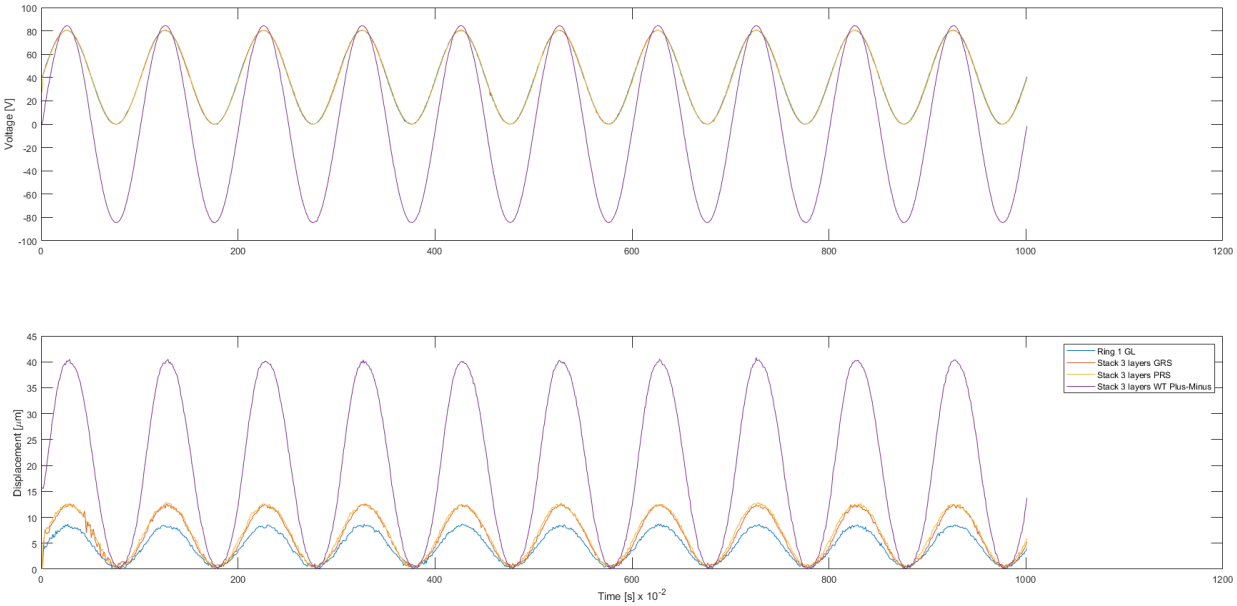

Fig. A.2: Ring 1 GL, Stack 3L GRS & PRS, WT Plus-Minus, single point, normalized by subtracting s_{min}.

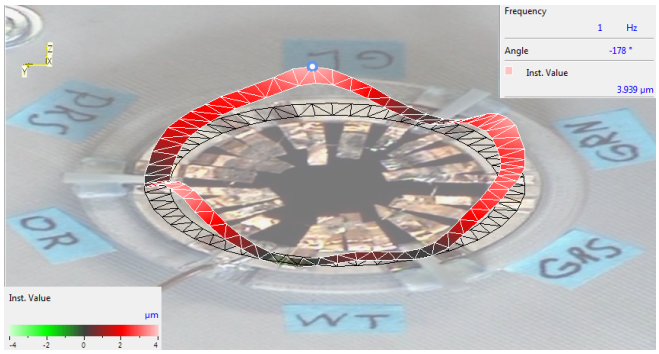

Fig. A.3: Ring 1, all segments active.

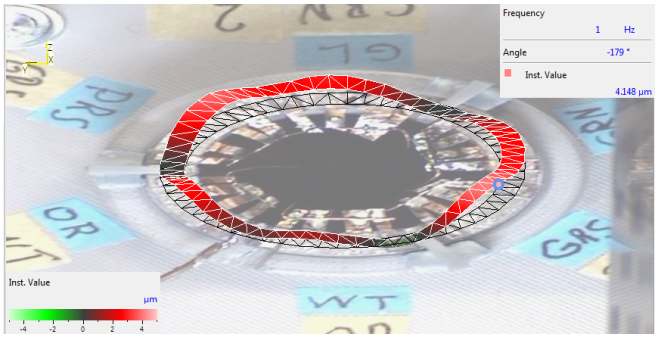

Fig. A.4: Ring 2, all segments active.

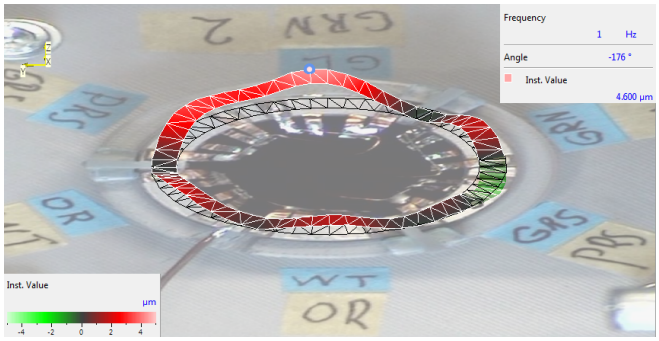

Fig. A.5: Ring 3, all segments active.

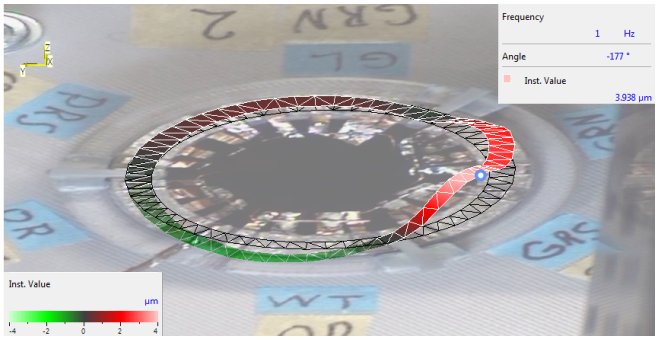

Fig. A.6: Ring 2, segments GL & PRS active.

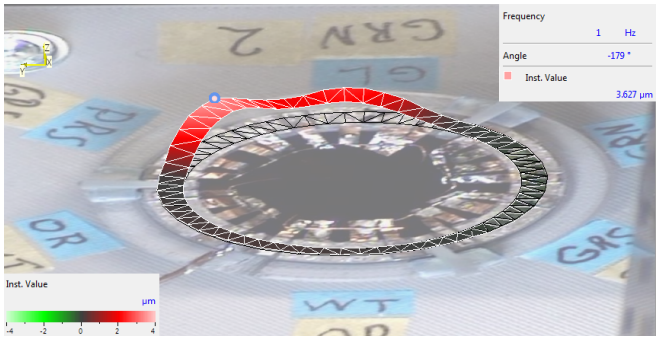

Fig. A.7: Ring 2, segments GRN & GRS active.

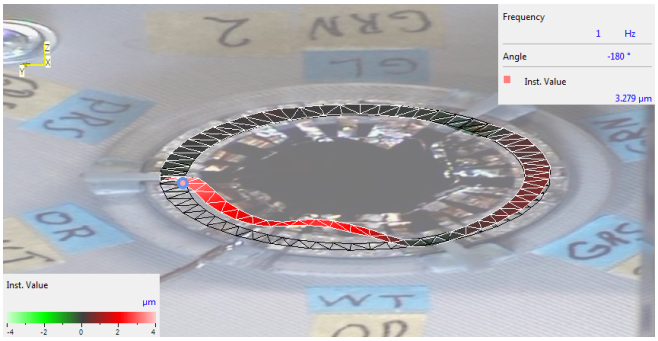

Fig. A.8: Ring 2, segments OR & WT active.

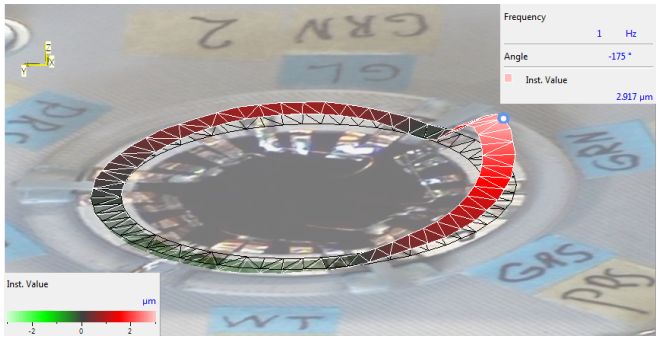

Fig. A.9: Ring 3, segment GL active.

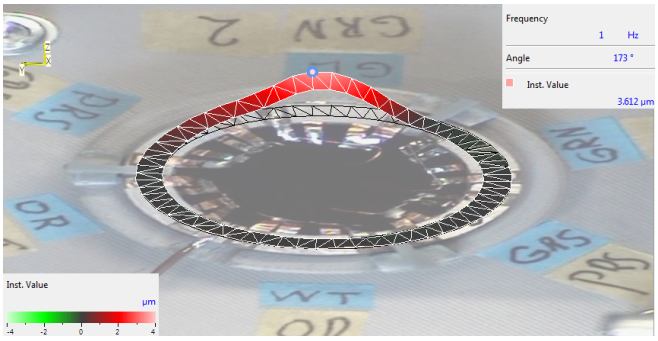

Fig. A.10: Ring 3, segment GRN active.

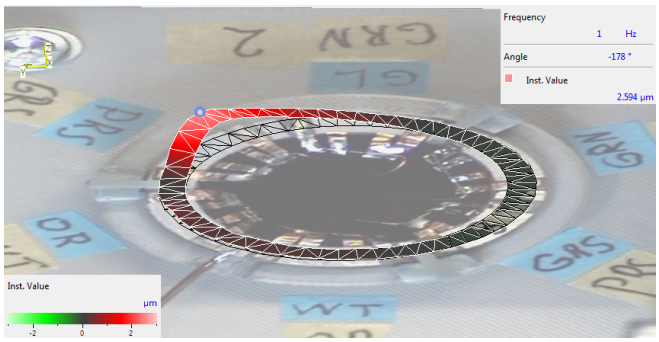

Fig. A.11: Ring 3, segment GRS active.

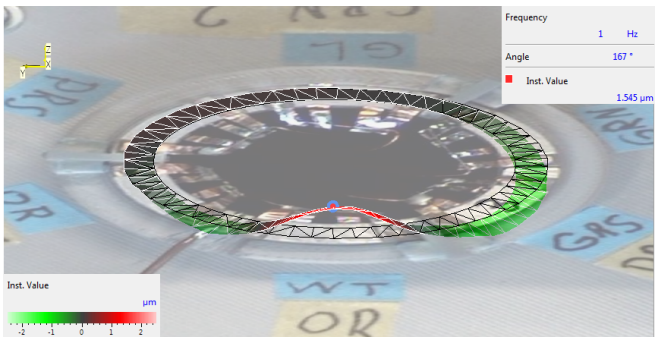

Fig. A.12: Ring 3, segment OR active.

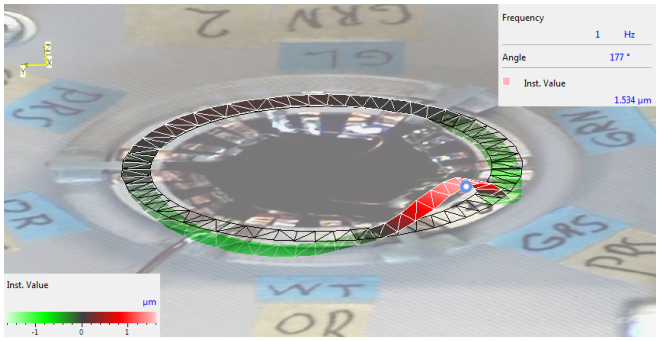

Fig. A.13: Ring 3, segment PRS active.

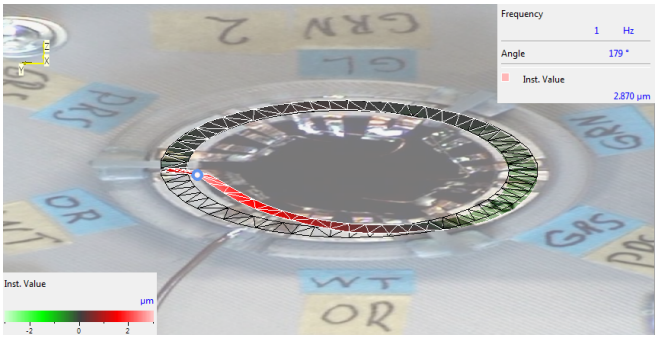

Fig. A.14: Ring 3, segment WT active.

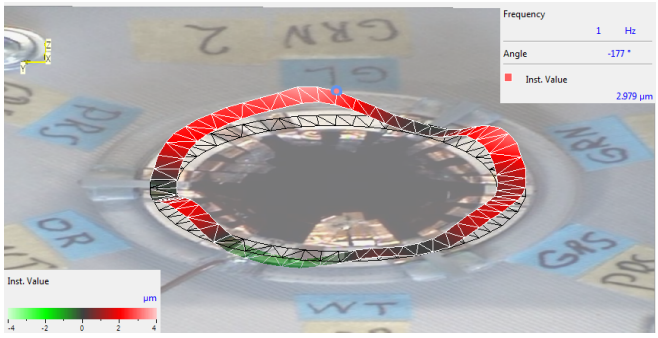

Fig. A.15: Stack, first layer, GL.

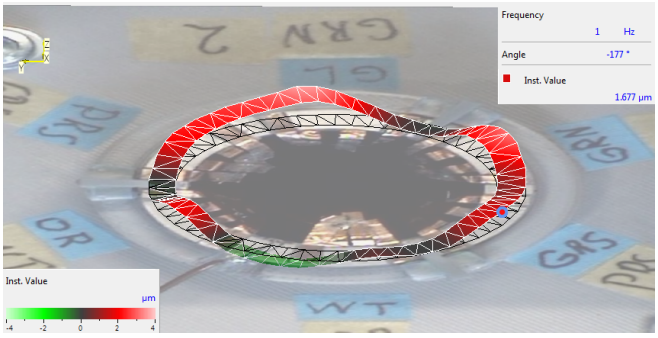

Fig. A.16: Stack, first layer, GRS.

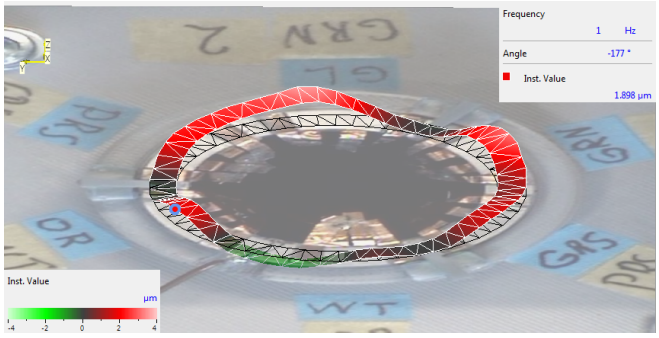

Fig. A.17: Stack, first layer, OR.

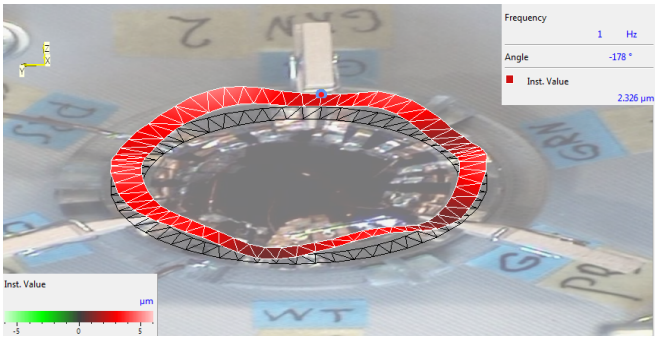

Fig. A.18: Stack, two layers, valley of connection 1.

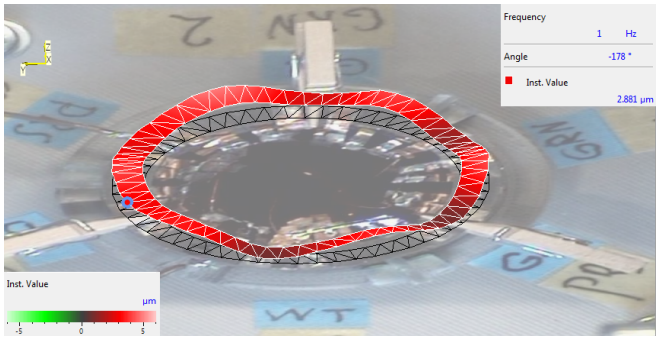

Fig. A.19: Stack, two layers, valley of connection 2.

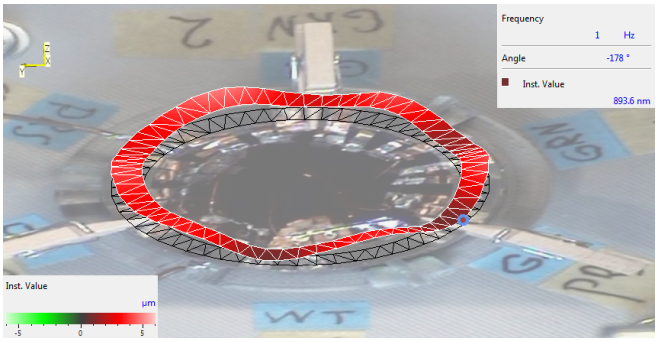

Fig. A.20: Stack, two layers, valley of connection 3.

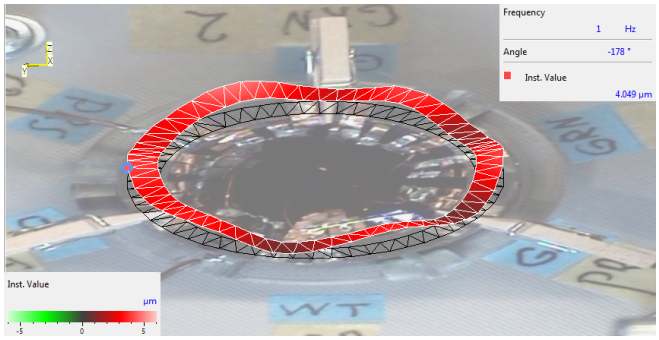

Fig. A.21: Stack, two layers, OR.

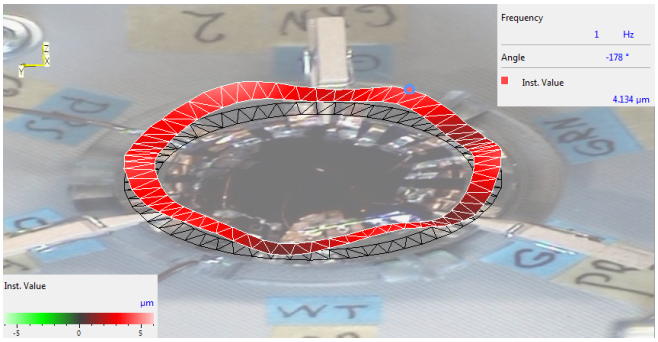

Fig. A.22: Stack, two layers, GRS.

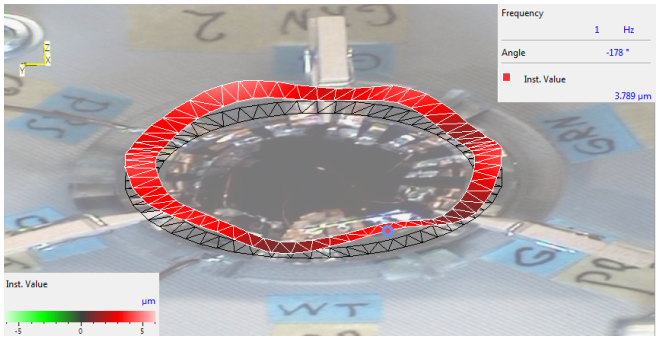

Fig. A.23: Stack, two layers, GL.

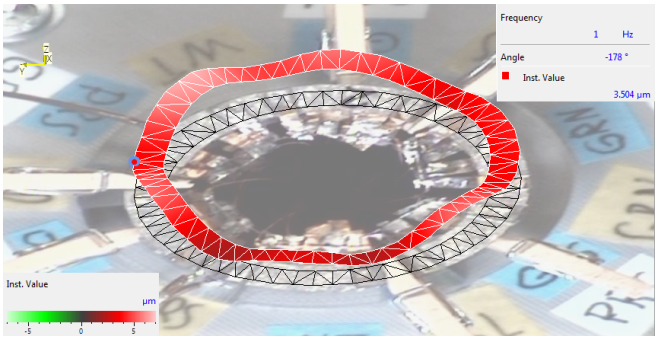

Fig. A.24: Stack, three layers, valley of connection 1.

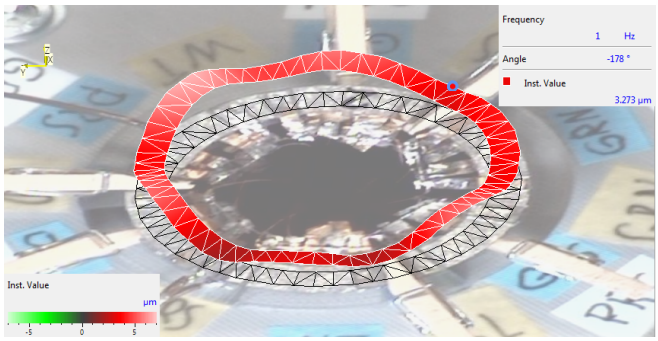

Fig. A.25: Stack, three layers, valley of connection 2.

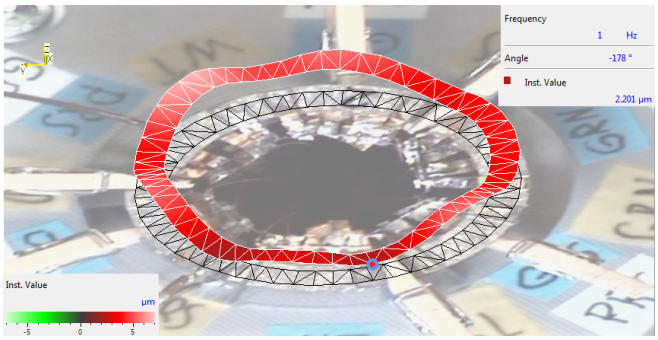

Fig. A.26: Stack, three layers, valley of connection 3.

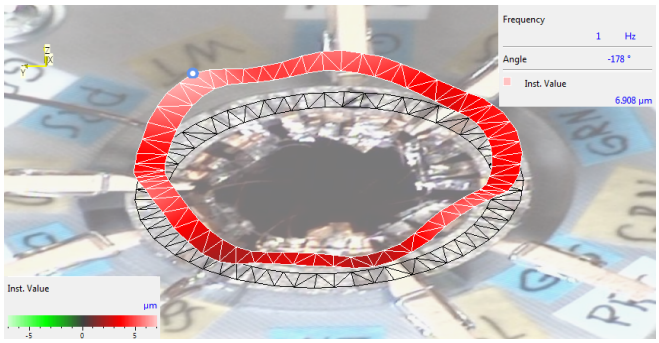

Fig. A.27: Stack, three layers, GRS.

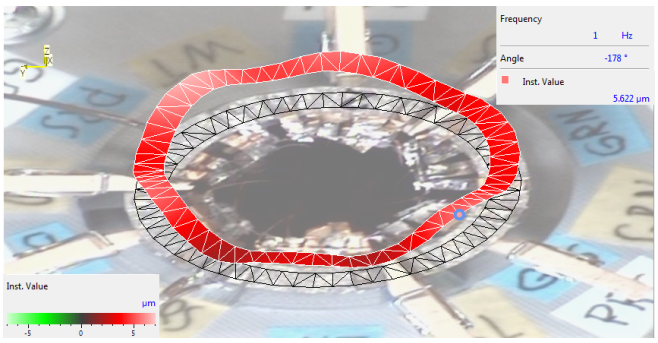

Fig. A.28: Stack, three layers, PRS.

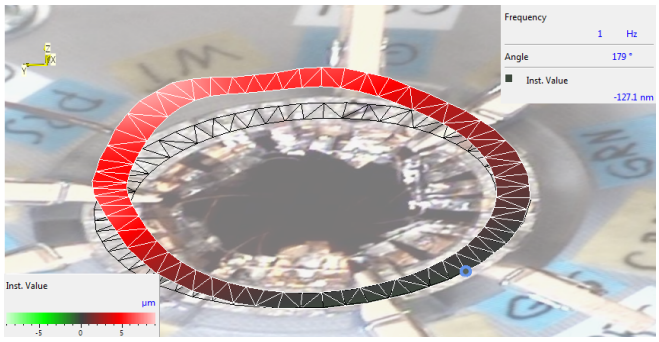

Fig. A.29: Stack, three layers, roll movement, valley.

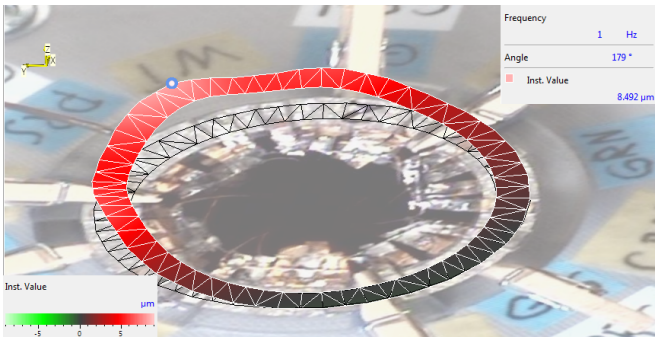

Fig. A.30: Stack, three layers, roll movement, peak.

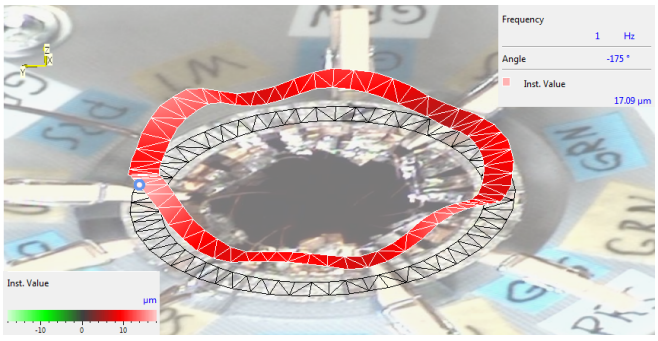

Fig. A.31: Stack, three layers, WT, $V_{min} = -84\,\mathrm{V}$ and $V_{max} = 84\,\mathrm{V}$.

4 Conclusion

The objectives of this study were (1) the employment of smart materials to make metamaterials active, (2) proposing a method of how to realize this using production materials and (3) employing these methods to build a small metamaterial demonstrator that functions both as the actuator and the structure. A literature review on electromechanical smart material transducers was conducted to (1) gain the knowledge that is critical for understanding the working principles of the transducers and (2) discover the potential for integrating smart material transducers in the unit cells of metamaterial. It is found that dielectric elastomers achieve high strains, low stress and need high driving voltages. Conducting polymers are able to deliver both high stress and high strain, but consume relatively much power. If power consumption is a priority, Electronic EAPs are preferred. PVDF does not excel on stress or strain, but is an overall good performer. The main paper presents the methodology for designing and constructing a tube shaped metamaterial demonstrator of a high precision positioning system. The 3D geometry of the metamaterial was built by layering planer pre-fabricated structures which use smart material for actuation. The concept of multiple actuators on the top and bottom of a ring was able to successfully create waves in a ring. Thereby the concept can be used to create vertical displacements and could be interesting for building positioning systems. The measured maximum amplitude of a single layer was 4.60 µm. Three rings were successfully stacked into a metamaterial which resulted in an increased range. The created metamaterial can both function as the structural backbone of the system as well as the actuation part. Next to the ability to create a vertical displacement, the metamaterial also proved capable of creating roll movement. This allows the metamaterial tube to bend itself in every wished way. The measured maximum amplitude of the stack was 6.91 µm. Roll movement of the top layer of the stack was achieved with a lowest point of -0.13 µm and a highest point of 8.49 µm. The system showed that smart materials are a suitable choice to make metamaterial active, and that active metamaterial could be produced using production material. The planar approach for design and fabrication, provides a relatively simple and fast method for building metamaterial in general.

5 Recommendations

The methodology that is presented allows for a relatively simple and fast production process of active metamaterial. This makes active metamaterial a more competitive option in many research problems and should lead to more implementations in designs. To encourage this, the planar design of active metamaterial should be further investigated and combined with control.

The locally tunable unit cells of active metamaterials could be ideal for absorbing high local impacts such as bullets. Planarly designing such a device could keep costs low and fabrication relatively simple. A controller could manage the collaboration off all unit cells to gradually absorb the energy and safely distribute it to the human body. The unit cell for such a project should be able to change its shape, stiffness and damping rapidly. Smart material actuators could provide the fast response that is needed to achieve this.

For future work on this particular design, it would be interesting to further study the characteristics of the metamaterial. For example, the tunability of the shape of the unit cells can be exploited to create a material with tunable damping and stiffness when it would be complemented with control. This project focused only on displacements of the active metamaterial setup. The layers are made up out of flexible material and the actuators are suitable for high bandwidth applications. This combination would make it interesting to study the dynamical behavior. The metamaterial proved very capable of roll movement as was discussed earlier in this section. It would be interesting to build a controller to control the movement of the material and study the performance on this matter. Improvements on the metamaterial can be made by changing the design for a specific goal, optimizing the alignment and clamping tool, the use of thicker spring steel and refinement of the spacers.

Further development of the alignment and clamping tool could provide more consistent placement of the actuators on the stainless steel rings. This would rule out a large amount of the uncertainties faced while interpreting the results. If the actuators are capable of bending thicker stainless steel rings, these rings could provide more stiffness to the setup. A demonstrator which deformations are visible with the naked eye could be designed by choosing different actuator material and pair it with a matching flexible sublayer. A higher stiffness of the setup would result in a relatively lower influence of the stiffness of the wires on the setup. Ideally the clamping points on the base should be as thin as possible. This way they will take up the least amount of torque, which will minimize the influence on the behavior of the ring. If dynamical behavior would be of interest, a more rigid connection between the rings would be preferred.

A File guide

Active Metamaterial Archive – *All the needed data to create active metamaterial*

- Calculations – *MATLAB files*
  - Displacement – *Modelling of the displacement*
  - Distribution – *How the actuators and spacers are distributed*
- Design – *SW files*
  - 3D printing – *SW for printing*
  - *Laser cutting – SW for laser cutting*
  - Assemblies & Models – *SW for visualization*
- Literature – *Papers, books, etc.*
  - Literature review – *Literature used during*
  - Research paper – *Literature used during*
- Presentations – *PowerPoints*
  - Literature – *Presentations given during*
  - Midterm – *Presentations given during*
- Results – *Results obtained*
  - LabVIEW – *Data from the single point setup*
  - MATLAB – *Processed data by MATLAB*
  - Report results – *Results that were used in the report*
  - Vibrometer – *Data from the multipoint setup*

Bibliography

[1] Milton, G. W., and Cherkaev, A. V. (October 1, 1995). "Which Elasticity Tensors are Realizable?." ASME. *J. Eng. Mater. Technol*. October 1995; 117(4): 483–493.

[2] Carneiro, V. H., Meireles, J., & Puga, H. (2013). Auxetic materials—A review. *Materials Science-Poland*, *31*(4), 561-571.

[3] Goldsberry, B. M., & Haberman, M. R. (2018). Negative stiffness honeycombs as tunable elastic metamaterials. *Journal of applied physics*, *123*(9), 091711.

[4] S. Theodossiades and S. Natsiavas, “Non-linear dynamics of gear-pair systems with periodic stiffness and backlash,” *Journal of Sound and vibration*, vol. 229, no. 2, pp. 287–310, 2000.

[5] R. Slatter and R. Degen, “Miniature zero-backlash gears and actuators for precision positioning applications,” in *Proc. of 11th European Space Mechanisms and Tribology Symposium ESMATS*, 2005, pp. 9–16.

[6] W. Huang, L. Cai, and X. Tang, “Adaptive repetitive output feedback control for friction and backlash compensation of a positioning table,” in *Proceedings of the 37th IEEE Conference on Decision and Control (Cat. No. 98CH36171)*, vol. 2. IEEE, 1998, pp. 1250–1251.

[7] G. P. Stachowiak, G. W. Stachowiak, and P. Podsiadlo, “Automated classification of wear particles based on their surface texture and shape features,” Tribology International, vol. 41, no. 1, pp. 34–43, 2008.

[8] Overvelde, J. T., De Jong, T. A., Shevchenko, Y., Becerra, S. A., Whitesides, G. M., Weaver, J. C., ... & Bertoldi, K. (2016). A three-dimensional actuated origami-inspired transformable metamaterial with multiple degrees of freedom. *Nature communications*, *7*(1), 1-8.

[9] Jothis, N. (2021). Active metamaterial unit cells incorporating piezoelectric actuator

[10] Thomas, D. (2020). Active metamaterials: unit cells for tunable damping.

[11] D. J. Leo, Engineering analysis of smart material systems. Wiley Online Library, 2007, vol. 435.

[12] P. J¨anker and W. Martin, Performance and characteristics of actuator materials. Deutsche Aerospace AG (DASA), 1993.